# RNA-protein interactome at the Hepatitis E virus internal ribosome entry site

Shiv Kumar[1], Rohit Verma[1], Sandhini Saha[2], Ashish Agrahari[3], Shivangi Shukla[1], Anurag[1], Tushar Kanti Maiti[2], Shailendra Asthana[3], C.T. Ranjith-Kumar[4], Milan Surjit[1]*

[1]Virology Laboratory, Translational Health Science and Technology Institute, NCR Biotech Science Cluster, Faridabad, 121001, Haryana, India.

[2]Laboratory of functional proteomics, Regional Centre for Biotechnology, NCR Biotech Science Cluster, Faridabad, 121001, Haryana, India.

[3]Noncommunicable disease group, Translational Health Science and Technology Institute, NCR Biotech Science Cluster, Faridabad, 121001, Haryana, India.

[4]University School of Biotechnology, Guru Gobind Singh Indraprastha University, New Delhi, 110078, India.

* Correspondence: milan@thsti.res.in

## Abstract

Multiple processes exist in a cell to ensure continuous production of essential proteins either through cap-dependent or cap-independent translation processes. Viruses depend on the host translation machinery for viral protein synthesis. Therefore, viruses have evolved clever strategies to utilize the host translation machinery. Earlier studies have shown that genotype 1-Hepatitis E virus (g1-HEV) utilizes both cap-dependent and cap-independent translation machineries for its replication and proliferation. Cap-independent translation in g1-HEV is driven by an eighty seven nucleotide-long RNA element which acts as a noncanonical, internal ribosome entry site like (IRESl) element. Here, we have identified the RNA-protein interactome of the HEV IRESl element and characterized the functional significance of some of its components. Our study reveals indispensable roles of host ribosomal protein RPL5 and DHX9 (RNA helicase A) in mediating efficient translation from the IRESl element and establish the function of HEV IRESl as a bonafide internal ribosome entry site.

## Author summary

Protein synthesis is a fundamental process for survival and proliferation of all living organisms. Majority of cellular proteins are produced through a cap-dependent translation process. However under conditions of stress and/or when cap-dependent translation is not operational, cells utilize a variety of cap-independent translation processes to synthesize essential proteins. Viruses are the only living organisms which depend on the host cell translation apparatus to synthesize their own proteins. Many viruses utilize both cap-dependent and cap-independent machineries for the synthesis of viral proteins. Hepatitis E virus is a major cause of acute hepatitis worldwide. The viral genome is a capped positive strand RNA. Viral non-structural and structural proteins are synthesized through a cap-dependent translation process from one open reading frame (ORF) present in the genomic RNA and two overlapping ORFs present in the subgenomic RNA, respectively. An earlier study from our laboratory reported the presence of a fourth ORF in the viral genome, which produced the ORF4 protein using a cap-independent internal translation initiation mechanism. Using bicistronic reporter assays and site-directed mutagenesis studies, it was demonstrated that translation of the ORF4 protein was driven by an internal ribosome entry site-like (IRESl) element. In the current study, we identified the host proteins that directly or indirectly associate with the HEV-IRESl RNA and generated the RNA-protein interactome. Subsequent studies identified essential roles of ribosome protein L5 (RPL5) and DHX9 (RNA Helicase A) in mediating the function of the IRESl. Biochemical fractionation studies showed the presence of IRESl and its components in the actively translating polysomes. Collectively, our data proves that HEV-IRESl is a bonafide internal ribosome entry site.

## Introduction

Protein synthesis is an essential process for survival and growth of all organisms. Viruses depend on the host cell machinery for synthesis of their proteins. Proteins are synthesized by the process of translation, which involves four distinct steps such as initiation, elongation, termination and recycling of the ribosomes. In eukaryotes, under normal conditions, majority of mRNA are translated by recognition of the $m^7G$ (5')$_{PPP}$(5')N(cap) structure present at the 5'-end of the mRNA, by the process of cap-dependent translation. Many cellular and viral mRNAs are translated by the cap-independent mechanisms, by using distinct *cis*-acting regulatory elements, such as the cap-independent translational enhancers (CITEs), $m^6A$ modification of the mRNAs or the internal ribosome entry sites (IRES). Initiation of the cap-dependent translation occurs through a ribosomal scanning mechanism, in which the 48S initiation complex moves along the mRNA from the $m^7G$ cap in the 5' to 3' direction to locate a suitable AUG initiation codon. Following AUG recognition, through a series of steps, 80S ribosome complex is assembled on the mRNA with met-tRNAi bound to the AUG codon at the P-site, leading to translation elongation (1). The CITES are located in either 5'- or 3'- UTRs (untranslated regions) of the mRNAs and they initiate cap-independent translation by recruiting the initiation factors to the uncapped mRNAs, followed by 5'-end ribosomal scanning mediated identification of the initiation codon. Under conditions of stress, the cap-independent translation of many cellular mRNAs such as c-myc, Apaf-1, XIAP seem to occur through the above mechanism (2,3). A variant of the eukaryotic initiation factor 4G (eIF4G) has been shown to be important for the cap-independent translation of the c-myc mRNA (4). Recently, yeast eIF4G1 was shown to mediate the cap-independent translation from the black beatle virus 5'-untranslated region (UTR) (5). Translation of 5'- or 3'- UTR $m^6A$ modified mRNAs also occur in a cap-independent manner (6,7,8).

Cap-independent, IRES-mediated translation has been reported in many positive-strand RNA viruses, which contain an uncapped genomic RNA. 5'-UTR in the genomic RNA of these viruses contain highly structured RNA elements, which directly recruit the initiation factors and promote translation through a scanning independent process, with the exception of the type I IRES, which depends on the ribosomal scanning process. IRES

109 have been divided into 5 major types based on their mode of ribosome recruitment and
110 RNA structure. The type I and type II IRES are found in the Picorna viruses such as the
111 Polio virus (PV) and the Foot and Mouth Disease virus (FMDV), respectively. The PV
112 IRES harbors six stem loops designated as domain I to VI. The Domain I forms unique
113 clover leaf structure and is critical for replication of both the positive and the negative
114 sense RNA. The domains II to VI are responsible for the PV IRES activity. During PV
115 infections, viral $2A^{pro}$ cleaves the eIF4E binding N-terminal domain of the eIF4G without
116 affecting its eIF3/eIF4A binding property. Stable association of the eIF4G with the PV
117 IRES domain V promotes binding of other initiation factors, leading to formation of the
118 43S preinitiation complex. The FMDV IRES is a well-studied example of the type II IRES.
119 The domain IV of the FMDV IRES binds with scaffold protein eIF4G**.** The $3C^{pro}$ and $L^{pro}$ of
120 FMDV cleave the eIF4G similar to the $2A^{pro}$ of the type I IRES**.** Notably, the FMDV IRES
121 skips ribosomal scanning, instead, IRES proximal stem loop formation brings 84
122 nucleotides downstream AUG, close to the first AUG to start the translation by direct
123 ribosome transfer**.** Other identified cis-acting elements for the type II IRES activity are the
124 GNRA, RAAA and C-rich loop in the domain III (9). The type III IRES is present in the 5'-
125 UTR of the Hepatitis A virus genome (10). It requires eIF4E binding for translation
126 initiation (11)**.** The type IV IRES have been reported in members of the Flaviviridae family,
127 classified as the HCV (Hepatitis C virus)/ HCV-like IRES. The 5'-UTR of HCV contains
128 four domains: the domain I and II are involved in the viral replication while the domains III
129 and IV are involved in the IRES activity (12,13). The HCV/HCV-like IRES are shorter in
130 comparison to the type I and II IRES. The domains II and III contain several subdomains
131 for interaction with the 40S ribosomal subunit. The type V IRES includes the long
132 intergenic region (IGR) IRES, found between two open reading frames in the viral
133 genomes and conserved in the dicistroviridae family (12,13). The IGR IRES are the
134 smallest IRES (~180 nt long) elements consisting of three pseudoknots. It directly binds
135 to the ribosomes and initiates translation with the alanine-tRNAi (ala-tRNAi) instead of the
136 met-tRNAi, without involving the eIFs (14,15).

137 Many viruses have evolved the ability to utilize both cap-dependent and cap-independent
138 translation processes, depending on the state of the cell. Notably, although Dengue virus
139 and Zika virus genomic RNA is usually translated through a cap-dependent mechanism,

140 their 5'-UTRs also contain IRES-elements, which maintain viral translation under
141 unfavorable conditions where cap-dependent translation is inhibited by the host
142 (16,17,18). Similarly, genomic RNA of the Human Immunodeficiency Virus (HIV) type 1
143 and the Simian Immunodeficiency virus (SIV) contain IRES-elements in their 5'-leader
144 sequences, which maintain viral translation when cap-dependent translation is inhibited
145 (19,20,21,22). In addition, recent studies have identified functional IRES elements within
146 open reading frames of viral protein coding genes. For example, five functional IRES-
147 elements are located within the coding region of the non-structural and the structural
148 proteins of the human rhinovirus 16, which are active under conditions of endoplasmic
149 reticulum (ER) stress (23,24). The Human cytomegalovirus pUL138 protein is translated
150 by an IRES under conditions of stress (25). Further, coat protein of the Turnip crinkle virus
151 (TCV) is translated through an unstructured IRES (26). Our earlier study demonstrated
152 the coexistence of both cap-dependent and cap-independent translation in the genotype
153 1-Hepatitis E Virus (g1-HEV) (27). Although HEV non-structural and structural proteins
154 are synthesized by a cap-dependent translation process, a protein essential for g1-HEV
155 replication (ORF4 protein) is synthesized from an overlapping ORF located within the viral
156 ORF1 through a cap-independent translation process. An 87 nucleotide conserved RNA
157 regulatory element located upstream of the ORF4 coding region was found to drive cap-
158 independent translation of the ORF4 protein. Interestingly, although ORF4 protein
159 production in g1-HEV infected cells was markedly enhanced upon treatment of cells with
160 ER stress-inducing compounds, HEV IRESl functioned efficiently irrespective of the ER
161 stress inducer treatment in *in-vitro* translation assays or bicistronic reporter based assays.
162 Analysis of cap-independent translation driven by the HEV RNA regulatory element by
163 bicistronic reporter assays along with site directed mutagenesis mediated mapping of the
164 regulatory RNA sequence suggested the HEV RNA regulatory element to be an IRES-
165 element. However, considering the small size of the regulatory element and its lack of
166 strong homology with canonical IRES-elements, it was designated as an IRES-like
167 (IRESl) element. The current study was designed to further explore the mechanism of
168 HEV IRESl activity and verify its function as a bonafide internal translation initiation site.
169 Host interaction partners of the HEV IRESl were identified and their importance in the
170 IRESl-mediated translation was evaluated. Subsequent experiments showed association

171 of the HEV IRESl RNA with actively translating ribosomes, supporting its role as a
172 translation initiation element. Significance of these findings in validating the role of HEV
173 IRESl as a bonafide internal ribosome entry site is discussed.

174

175 **Results**

176 **Identification of host proteins that interact with the HEV IRESl element**

177 Two independent experimental approaches (RaPID assay and Yeast three hybrid assay)
178 were followed to identify the host proteins that interact with the HEV IRESl RNA. RNA -
179 protein interaction detection assay (RaPID assay) involves biotinylation of IRES
180 interacting proteins, followed by their identification by liquid chromatography with tandem
181 mass spectroscopy (LC-MS-MS) (28). RaPID assay was optimized in our laboratory (29).
182 87 nucleotides of the g1-HEV genome (Genbank ID: AF444002.1) corresponding to the
183 IRESl region was cloned into the pRMB vector between the BirA ligase binding stem-loop
184 (RMB-SLI, RMB-SLII) sequences (Fig. 1A, 1C). Analysis of the secondary structure of the
185 fusion RNA sequence using “Mfold” indicated that the HEV IRESl and the BirA ligase
186 binding stem-loops retained their distinct folding characteristics (Fig. 1A). An unrelated
187 sequence in the g1-HEV genome (618-738 nucleotides from the 5’-end) was also cloned
188 into the pRMB vector to be used as a control to monitor specificity of the assay. Biotin-
189 untreated cells were used as an additional control and experiments were performed two
190 times and samples of each experiment were run in triplicate.

191

Figure 1

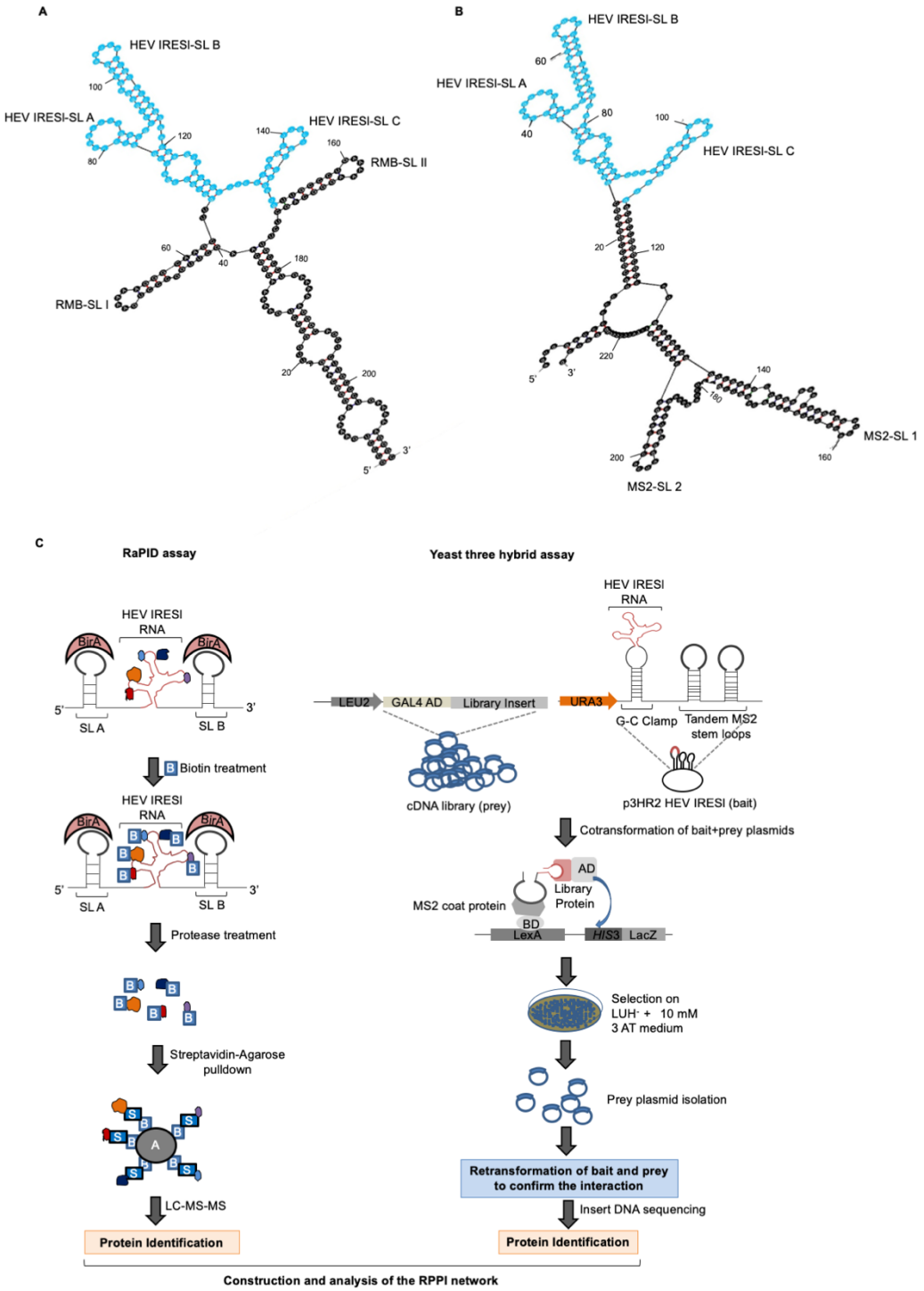
A
HEV IRESI-SL B
HEV IRESI-SL A
HEV IRESI-SL C
RMB-SL II
RMB-SL I
B
HEV IRESI-SL B
HEV IRESI-SL A
HEV IRESI-SL C
MS2-SL 1
MS2-SL 2
C
RaPID assay
Yeast three hybrid assay
HEV IRESI RNA
BirA
SL A
SL B
Biotin treatment
Protease treatment
Streptavidin-Agarose pulldown
LC-MS-MS
Protein Identification
LEU2
GAL4 AD
Library Insert
URA3
G-C Clamp
Tandem MS2 stem loops
cDNA library (prey)
p3HR2 HEV IRESI (bait)
Cotransformation of bait+prey plasmids
AD
Library Protein
MS2 coat protein
BD
LexA
HIS3
LacZ
Selection on LUH⁻ + 10 mM 3 AT medium
Prey plasmid isolation
Retransformation of bait and prey to confirm the interaction
Insert DNA sequencing
Protein Identification
Construction and analysis of the RPPI network

192

193 **Figure 1. Identification of host interaction partners of the HEV IRESl element by**
194 **RaPID and Yeast three hybrid assay.**
195 (A) Schematic of predicted secondary structure of the HEV IRESl RNA (highlighted in blue) fused
196 to the BirA-binding RNA motifs (RMB-SL1 and RMB-SL2). Stem-loops of the HEV IRESl are
197 denoted as SL A, SL B, SL C (B) Schematic of predicted secondary structure of the HEV IRESl
198 RNA (highlighted in blue) fused to the MS2 coat protein-binding RNA motifs (MS2-SL1 and MS2-
199 SL2). Stem-loops of the HEV IRESl are denoted as SL A, SL B, SL C (C) Work-flow to identify
200 the HEV IRESl-binding host proteins. B: Biotin, A: Agarose, S: Streptavidin, AD: GAL4-Activation
201 domain, BD: GAL4-DNA Binding domain, L: Leucine, U: Uracil, H: Histidine, 3-AT: 3-Amino 1, 2,
202 4 Triazole, "−": Deficiency in the medium, "+": Supplemented in the medium.

203

204 Quality of the MS data between replicates of different samples was checked by Pearson
205 correlation analysis, which showed good correlation (average range: 0.2-1.0). Proteins
206 with at least one biotinylated peptide with PEP (posterior error probability) score ≥ the
207 median value in the Gaussian smoothing curve of each sample were selected for further
208 analysis. Specific interaction partners of the HEV IRESl RNA was selected by subtracting
209 the biotinylated HEV IRESl data set from the biotinylated HEV (618-738), unbiotinylated
210 HEV (618-738) and unbiotinylated HEV IRESl datasets (Fig. 2A, Fig. S1, Table S1). The
211 HEV IRESl RNA-binding protein dataset thus obtained was further analyzed to select only
212 those proteins that were represented by a minimum of one unique peptide and a "prot
213 score" of 30 or more. Thus, a total of 43 unique proteins were identified as interaction
214 partners of the HEV IRESl RNA (Fig. 2B, Table 1).

215

**Figure 2**

A

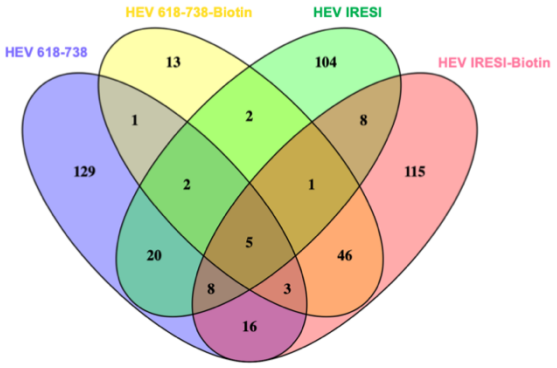


B

No. of HEV IRESI-interacting unique proteins (RaPID assay) : 43

No. of HEV IRESI-interacting unique proteins (Y3H assay) : 8

Total No. of HEV IRESI-interacting unique proteins : 51

C

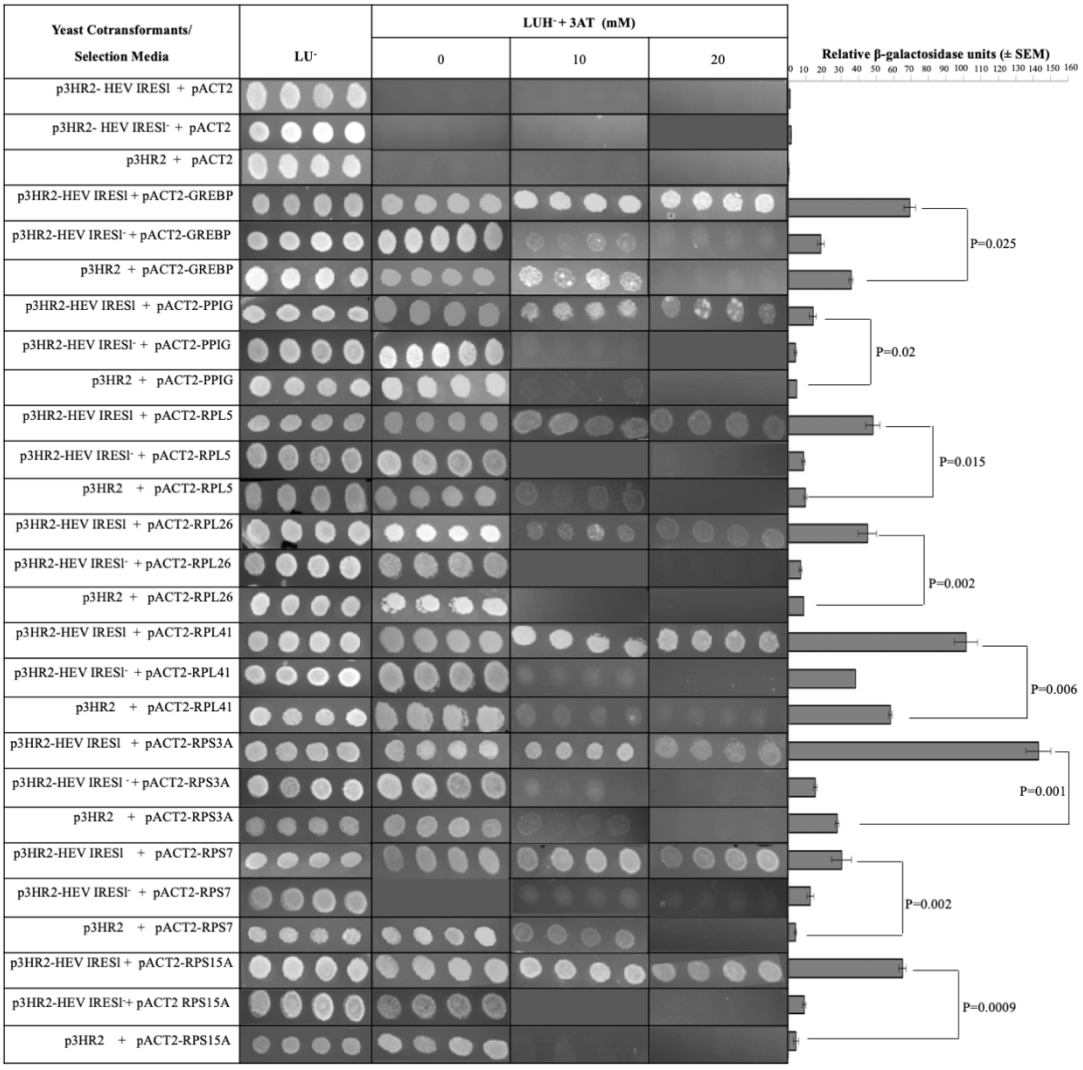


216

217 **Figure 2. Identification of HEV IRESl RNA-binding proteins by RaPID and Y3H**
218 **assay.**

219 (A) Venny analysis of the HEV IRESl RNA-binding proteins identified by the RaPID assay.
220 (B) Summary of the HEV IRESl RNA-binding proteins identified by the RaPID and the
221 Y3H assay. (C) Y3H assay mediated confirmation of the interaction between HEV IRESl
222 RNA and the host proteins identified by screening of the human liver cDNA library. YBZ1
223 strain was transformed in the indicated combinations and plated on media lacking Leucine
224 and Uracil ($LU^-$ ). Four random colonies from each cotransformant plate were replica
225 plated onto media lacking Leucine, Uracil, Histidine ($LUH^-$ ) and supplemented with 5mM
226 or 10mM 3-amino 1, 2, 4 Triazole (3-AT). Same colonies were used in liquid β-
227 galactosidase assay. Relative β-galactosidase units are plotted as mean (± SEM).

228

229

230

231

232

233

234

235

236

237

238

239

240

241 **Table 1. Host interaction partners of the HEV IRESI element**

| Gene name | Description | Prot_score | No. of biotinylated peptide | No. of unique biotinylated peptide |
|---|---|---|---|---|
| **(A) HEV IRESI-interacting host proteins, identified by the RaPID assay[a]** | | | | |
| *EEF2* | Elongation factor 2 | 1568 | 8 | 6 |
| *TUBA3C* | Tubulin alpha-3C/D chain | 929 | 1 | 1 |
| *HNRNPA2B1* | Heterogeneous nuclear ribonucleoproteins A2/B1 | 338 | 2 | 2 |
| ***DHX9*** | ATP-dependent RNA helicase A | 285 | 8 | 7 |
| *TARS* | Threonyl-tRNA synthetase, cytoplasmic | 285 | 7 | 5 |
| *RPL7A* | 60S ribosomal protein L7a | 262 | 4 | 3 |
| *BAT2L2* | Protein BAT2-like 2 | 75 | 1 | 1 |
| *NUFIP2* | Nuclear fragile X mental retardation-interacting protein 2 | 75 | 2 | 1 |
| *VARS* | Valyl-tRNA synthetase | 56 | 12 | 8 |
| *ARPP19* | cAMP-regulated phosphoprotein 19 | 53 | 1 | 1 |
| *ENSA* | Alpha-endosulfine | 53 | 1 | 1 |
| *RPL24* | 60S ribosomal protein L24 | 53 | 1 | 1 |
| *TARSL2* | Probable threonyl-tRNA synthetase 2, cytoplasmic | 53 | 5 | 5 |
| *YTHDF2* | YTH domain family protein 2 | 53 | 3 | 2 |
| *HSPH1* | Heat shock protein 105 kDa | 50 | 9 | 6 |
| *CAT* | Catalase | 49 | 2 | 2 |
| *DDX10* | Probable ATP-dependent RNA helicase DDX10 | 42 | 15 | 9 |
| *LARP4* | La-related protein 4 | 42 | 6 | 1 |
| *NDUFAF2* | Mimitin, mitochondrial | 41 | 1 | 1 |
| *DBNL* | Drebrin-like protein | 39 | 3 | 1 |
| *LBR* | Lamin-B receptor | 38 | 1 | 1 |
| *NSF* | Vesicle-fusing ATPase | 37 | 1 | 1 |
| *CEACAM16* | Carcinoembryonic antigen-related cell adhesion molecule 16 | 35 | 1 | 1 |
| *VWA5B1* | von Willebrand factor A domain-containing protein 5B1 | 35 | 5 | 5 |
| *CCDC65* | Coiled-coil domain-containing protein 65 | 34 | 5 | 5 |
| *PUM1* | Pumilio homolog 1 | 34 | 4 | 2 |
| *ARSJ* | Arylsulfatase J | 33 | 2 | 1 |
| ***RPA1*** | Replication protein A 70 kDa DNA-binding subunit | 33 | 4 | 4 |
| *TXLNG* | Gamma-taxilin | 33 | 17 | 10 |
| *AIMP1* | Aminoacyl tRNA synthetase complex-interacting multifunctional protein 1 | 32 | 5 | 3 |
| *BIVM* | Basic immunoglobulin-like variable motif-containing protein | 32 | 7 | 3 |
| *CCDC67* | Coiled-coil domain-containing protein 67 | 32 | 8 | 8 |
| *RSBN1L* | Round spermatid basic protein 1-like protein | 32 | 1 | 1 |
| *SH3PXD2A* | SH3 and PX domain-containing protein 2A | 32 | 1 | 1 |
| *UBAP2* | Ubiquitin-associated protein 2 | 32 | 2 | 1 |
| *GLS* | Glutaminase kidney isoform, mitochondrial | 31 | 6 | 1 |
| *MRE11A* | Double-strand break repair protein MRE11A | 31 | 1 | 1 |
| *ARL6IP5* | PRA1 family protein 3 | 31 | 2 | 1 |
| *CENPP* | Centromere protein P | 30 | 2 | 1 |
| *ERP29* | Endoplasmic reticulum resident protein 29 | 30 | 2 | 1 |
| *LASP1* | LIM and SH3 domain protein 1 | 30 | 1 | 1 |
| *TMEM59L* | Transmembrane protein 59-like | 30 | 2 | 1 |
| **(B) HEV IRESI-interacting host proteins, identified by the Y3H assay** | | | | |
| *GREBP* | cGMP-response Element–binding protein | | | |
| *PPIG* | Peptidylprolyl Isomerase G | | | |
| *RPL5* | Ribosomal protein L5 | | | |
| ***RPL26*** | Ribosomal protein L26 | | | |
| *RPL41* | Ribosomal protein L41 | | | |
| ***RPS3A*** | Ribosomal protein S3A | | | |
| *RPS7* | Ribosomal protein S7 | | | |
| *RPS15A* | Ribosomal protein S15A | | | |

242 [a]RaPID data has been sorted on the basis of Prot score

243 As an alternative approach to unbiasedly identify the protein interaction partners of the
244 HEV IRESl RNA, a human liver cDNA library was screened using the yeast three hybrid
245 (Y3H) assay (Fig. 1C) (30,31). In Y3H assay, the bait RNA is flanked by two copies of the
246 MS2-coat protein-binding RNA element. Analysis of the RNA sequence containing fusion
247 of the HEV-IRESl RNA and the MS2-coat protein binding stem loop RNA sequences
248 using "Mfold" indicated that their secondary structure profiles remain unaltered in the
249 fusion RNA( Fig. 1B). Self-activation of the *lacZ* and *HIS3* reporter genes by the HEV
250 IRESl RNA was checked by cotransforming the plasmids encoding the HEV IRESl (
251 p3HR2-HEV IRESl) and the GAL4 activation domain (pACT2) into chemically competent
252 YBZ1 yeast cells, followed by selection of the cotransformants on the $LUH^-$ medium and
253 assay of the β-galactosidase activity. No growth of colonies were seen on the $LUH^-$ plates
254 neither β-galactosidase activity was observed, indicating that there was no self-activation
255 of the reporter genes by the bait RNA (Fig. 2C). Next, the bait RNA expressing YBZ1 cells
256 were transformed with the human liver cDNA library. A total of $4x10^6$ clones were
257 screened and cotransformants were selected on the $LUH^-$ medium supplemented with
258 10mM 3-amino 1,2,4 triazole(3-AT). Note that 3-AT is a competitive inhibitor of the
259 Histidine biosynthesis pathway. Therefore, addition of 3-AT allows growth of the
260 cotransformants that show strong interaction between the bait RNA and the prey protein.
261 395 colonies were obtained in the primary screening, out of which human liver cDNA
262 insert could be detected in 285 colonies (Table S2). Restriction pattern analysis of the
263 prey plasmid DNA isolated from the 285 colonies showed that unique cDNA insert was
264 present in 75 plasmids. Analysis of the cDNA insert sequences identified 8 protein coding
265 genes, which were in frame with the GAL4 activation domain (Table S2).
266 Retransformation of those 8 plasmids along with the p3HR2-HEV IRESl plasmid showed
267 that all of them were able to interact with the HEV IRESl (Fig. 2C). The eight proteins
268 include 6 ribosomal proteins (RPL5, RPL26, RPL41, RPS3A and RPS7, RPS15A), PPIG
269 (peptidylprolyl isomerase G) and GREBP (cyclic-GMP response element binding protein)
270 (Table 1).

271 Further, specificity of the interaction of eight Y3H-identified proteins with the HEV IRESl
272 was evaluated in two ways: (a) by measuring the interaction of those proteins with an
273 RNA sequence complementary to the HEV IRESl (HEV $IRESl^-$) (b) by measuring the

274 interaction of those proteins with the known IRES sequences from the genotype 3A
275 Hepatitis C virus (HCV) and the foot and mouth disease virus (FMDV). All sequences
276 were cloned into the p3HR2 vector, upstream of the MS2 coat protein-binding stem-loop
277 RNA sequences (Fig. S2). No significant interaction was observed between HEV IRESI-
278 RNA and the host proteins (Fig. 2C). Y3H analysis revealed that only RPS3A interacts
279 with equal strength with all the three RNA sequences (HEV IRESI, FMDV IRES, HCV
280 IRES) (Table S3 and Fig. 3). RPL41 and RPS15A interacts exclusively with the HEV
281 IRESI RNA. While, RPL5 and RPS7 were found to interact strongly with the HEV IRESI
282 RNA and weakly with the HCV IRES. RPL26 interacts moderately and strongly with the
283 HEV IRESI and the HCV IRES, respectively, whereas it did not interact with the FMDV
284 IRES. GREBP interacts strongly with the HEV IRESI and weakly with both FMDV IRES
285 and HEV IRESI. PPIG also showed a difference in the strength of interaction among the
286 three RNA sequences in the following order- HCV IRES: strong interaction, HEV IRESI:
287 weak interaction and FDMV IRES: no interaction (Table S3 and Fig. 3).

288

**Figure 3**

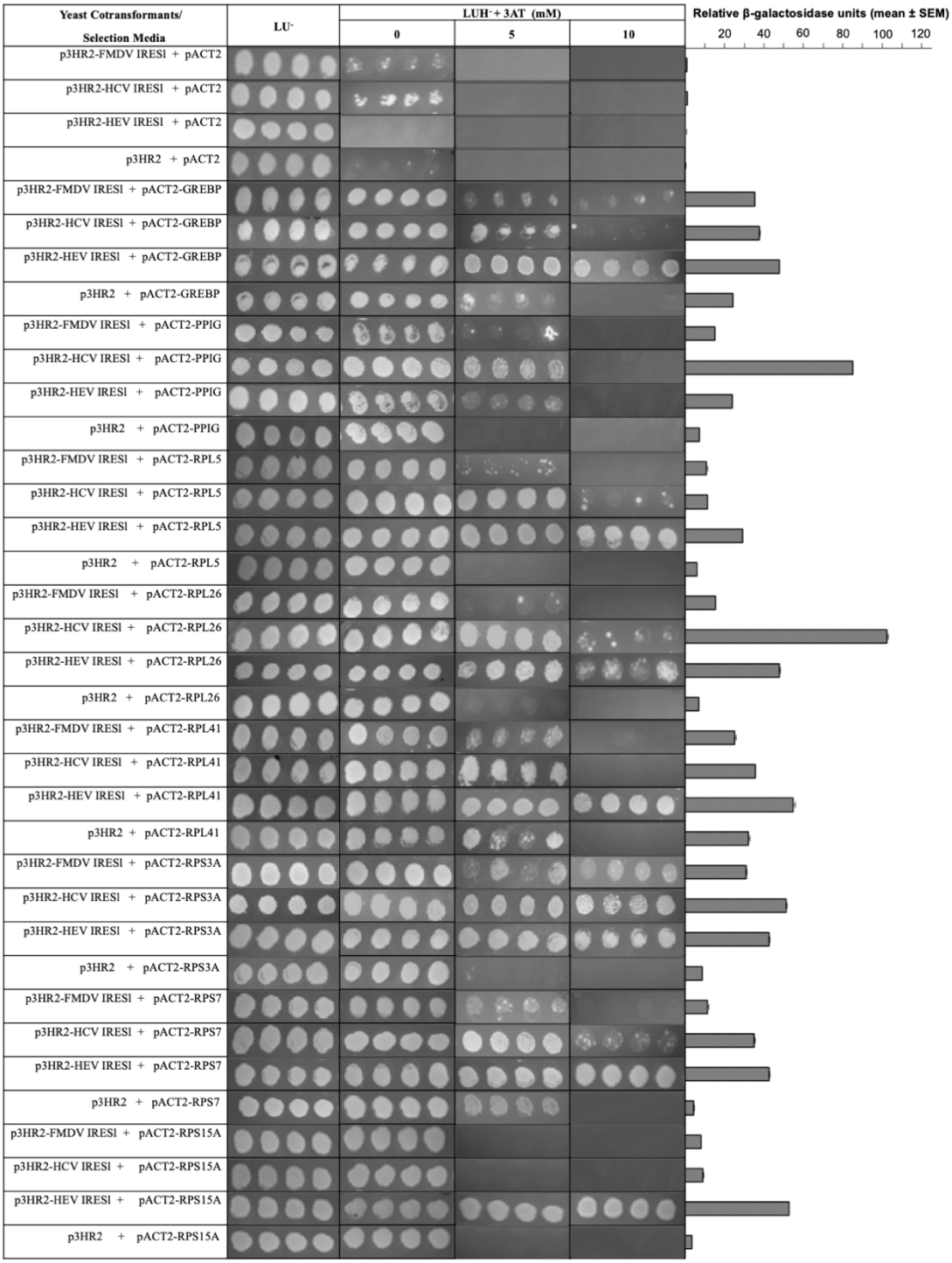
Yeast Cotransformants/
Selection Media
LU-
LUH- + 3AT (mM)
0
5
10
Relative β-galactosidase units (mean ± SEM)
20
40
60
80
100
120
p3HR2-FMDV IRESl + pACT2
p3HR2-HCV IRESl + pACT2
p3HR2-HEV IRESl + pACT2
p3HR2 + pACT2
p3HR2-FMDV IRESl + pACT2-GREBP
p3HR2-HCV IRESl + pACT2-GREBP
p3HR2-HEV IRESl + pACT2-GREBP
p3HR2 + pACT2-GREBP
p3HR2-FMDV IRESl + pACT2-PPIG
p3HR2-HCV IRESl + pACT2-PPIG
p3HR2-HEV IRESl + pACT2-PPIG
p3HR2 + pACT2-PPIG
p3HR2-FMDV IRESl + pACT2-RPL5
p3HR2-HCV IRESl + pACT2-RPL5
p3HR2-HEV IRESl + pACT2-RPL5
p3HR2 + pACT2-RPL5
p3HR2-FMDV IRESl + pACT2-RPL26
p3HR2-HCV IRESl + pACT2-RPL26
p3HR2-HEV IRESl + pACT2-RPL26
p3HR2 + pACT2-RPL26
p3HR2-FMDV IRESl + pACT2-RPL41
p3HR2-HCV IRESl + pACT2-RPL41
p3HR2-HEV IRESl + pACT2-RPL41
p3HR2 + pACT2-RPL41
p3HR2-FMDV IRESl + pACT2-RPS3A
p3HR2-HCV IRESl + pACT2-RPS3A
p3HR2-HEV IRESl + pACT2-RPS3A
p3HR2 + pACT2-RPS3A
p3HR2-FMDV IRESl + pACT2-RPS7
p3HR2-HCV IRESl + pACT2-RPS7
p3HR2-HEV IRESl + pACT2-RPS7
p3HR2 + pACT2-RPS7
p3HR2-FMDV IRESl + pACT2-RPS15A
p3HR2-HCV IRESl + pACT2-RPS15A
p3HR2-HEV IRESl + pACT2-RPS15A
p3HR2 + pACT2-RPS15A

289

290 **Figure 3. Assessment of the ability of the HEV IRESl-binding host proteins**
291 **(identified by the human liver cDNA library screening) to interact with the HCV IRES**
292 **and the FMDV IRES.**

293 YBZ1 strain was transformed in the indicated combinations and plated on media lacking
294 Leucine and Uracil ($LU^-$ ). Four random colonies from each cotransformant plate were
295 replica plated onto media lacking Leucine, Uracil, Histidine ($LUH^-$ ) and supplemented
296 with 5mM or 10mM 3-amino 1, 2, 4 Triazole (3-AT). Same colonies were used in liquid β-
297 galactosidase assay. Relative β-galactosidase units are plotted as mean (± SEM).

298

299 **Construction of the HEV IRESl RNA-host protein interaction network and analysis**
300 **of the interactome.**

301 43 and 8 host proteins identified as interaction partners of the HEV-IRESl RNA by RaPID
302 and Y3H assay, respectively, were clubbed and imported to Cytoscape to generate the
303 RNA-Protein-Protein interaction (RPPI) network, as described earlier (29). Analysis of the
304 different network characteristics revealed that the HEV IRESl-RPPI network contained 51
305 nodes and 74 edges, the average node degree being 3.36. Average clustering coeffient
306 was 0.44 and the PPI enrichment P-value was $1.11e^{-16}$ (Fig. 4A). Above network
307 parameters suggest that the HEV IRESl-RPPI network is highly connected and suitable
308 for further downstream studies.

309 Next, Gene ontology (GO) and Reactome pathway analysis of the HEV IRESl-RPPI
310 network was performed using the "Enrichr" tool to determine the significantly enriched
311 processes/pathways. Proteins involved in translation and mRNA catabolic processes
312 were enriched in the GO biological processes category, supporting involvement of the
313 HEV IRESl element in the protein synthesis process (Fig. 4B, top 10 biological processes
314 are shown). Similarly, top Reactome pathways include translation, eukaryotic translation
315 elongation and seleno animo acid metabolism (Fig. 4C, top 10 Reactome pathways are
316 shown). Analysis of the dataset using the gene set enrichment analysis (GSEA) tool also
317 showed translation and peptide metabolic process as top hits, in agreement with the
318 "Enrichr" output (Fig. S3A, S3B). Components of both small and large subunits of the

ribosome such as RPS7, RPS3A, RPS15A and RPL5, RPL24, RPL26, RPL41 interact with the HEV IRESl. Components of the tRNA synthetase complex such as Threonyl-tRNA synthetase (TARS), Valyl-tRNA synthetase(VARS), Aminoacyl tRNA synthetase complex-interacting multifunctional protein 1 (AIMP1) and a component of the translation elongation complex (EEF2, eukaryotic elongation factor 2) also interact with the HEV IRESl, further supporting its involvement in the protein synthesis process (Table 1). In addition, a literature search of IRES-binding host proteins revealed that four proteins identified in our study are known to bind other IRES. DHX9 and RPA1 bind to the IRES of HCV and FMDV; RPS3A associates with the HCV IRES, while RPL26 interacts with the p53 IRES (Table 1, highlighted in bold font) (32,33,34).

**Figure 4**

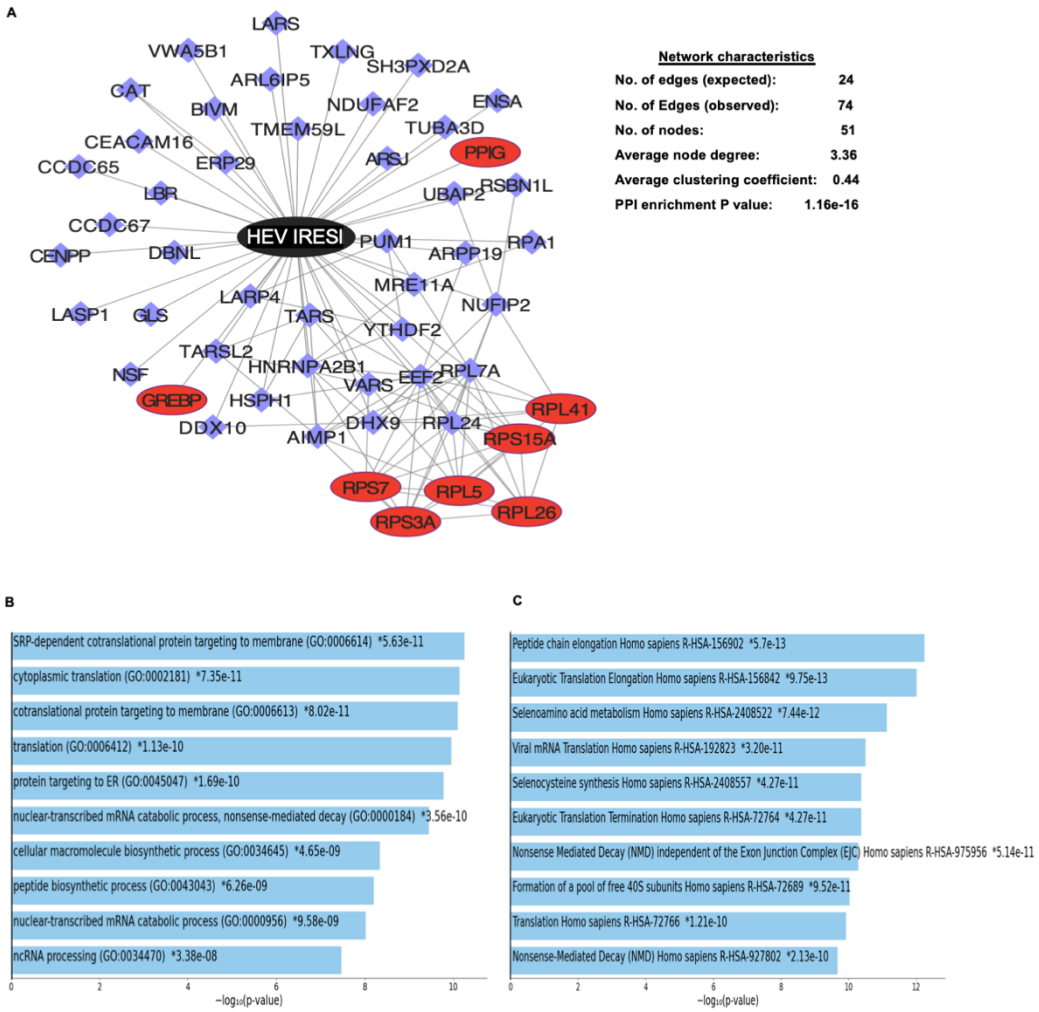

330 **Figure 4. Construction and analysis of the HEV IRESl RNA-protein interactome.**

331 (A) Schematic of the HEV IRESl RNA-protein interactome. Black node denotes HEV
332 IRESl RNA, blue and red nodes denote host proteins identified by the RaPID and the Y3H
333 assay, respectively. Edges are represented by blue lines (B) Graphical representation of
334 the top 10 Biological processes (sorted by *P*-values) enriched in the HEV IRESl RNA-
335 protein interactome (C) Graphical representation of the top 10 Reactome pathways
336 (sorted by *P*-values) enriched in the HEV IRESl RNA-protein interactome.

337

338 **Interrogation of the interaction between the HEV IRESl RNA and the host ribosomal**
339 **proteins by *in silico* analyses.**

340 *In silico* molecular docking has been used in determining the complex structures of RNA-
341 proteins interactions (35). We used HDOCK, a web-based tool which is a hybrid docking
342 algorithm of template-based modeling for determining the interaction between the HEV
343 IRESl RNA and four of the identified proteins (RPL5, RPL 26, RPS3A and RPS7) (36).
344 HEV IRESl showed direct interaction with RPL5, RPL26, RPS3A and RPS7 proteins (Fig.
345 5A-5D). All four complexes were analyzed for identification of the hot-spot residues and
346 was compared based on interaction mapping and binding energy analysis. All four
347 complexes were quantified in terms of their interaction by mapping the critical polar
348 contacts. The key nucleotides of each complex were mapped and, notably, RPS3A,
349 RPL26 and RPL5 were found to interact with the HEV IRESl through a combination of
350 common and unique nucleotides. The nucleotides U60, U29, G30 and U59 were common
351 in at least two complexes. The unique nucleotides which contribute significantly in RPL5
352 are G50 and C44; U22, G51 and C68 in RPS3A; A38, C41 and U66 in RPL26; U9, C10,
353 G12, G53 and G56 in RPS7 (Fig. 5E-5H). We also quantified the overall contributions by
354 measuring the surface contacts between the HEV IRESl nucleotides and proteins (Fig.
355 S3C). Here, the main focus was to identify the common nucleotides, which were involved
356 in contacts with the amino acids of the different ribosomal proteins. Interestingly, we found
357 that nucleotides A8, U9, C28, G51, G52, U59, U60, G61, U67, C68 and C69 were
358 common in at least three proteins. Nucleotides U29, G30, G31, A38, C41, A42, G50, C55,

359 A57, U62 and A85 were common among two proteins (Fig. S3C). Among the identified
360 nucleotides, some are engaged with two or more amino acids such as C10, U22, U29,
361 G30, U59 and U60, indicating their importance in mediating the interaction of the HEV
362 IRESl RNA with the respective ribosomal protein (Fig. 5E-5H). Further investigation of the
363 binding energy of each complex, the order of binding affinity between the four complexes
364 are RPL5 (-391.48 kcal/mol), RPL26 (-363.43 kcal/mol), RPS3A (-341.19 kcal/mol) and
365 RPS7 (-302.44 kcal/mol) (Fig. 5I). Physico-chemical analysis of the interacting amino
366 acids, it was observed that most of the interacting residues were either basic (K/R) or
367 aromatic (Y/F/H) in nature and each complex involves at least one serine residue.

368

**Figure 5**

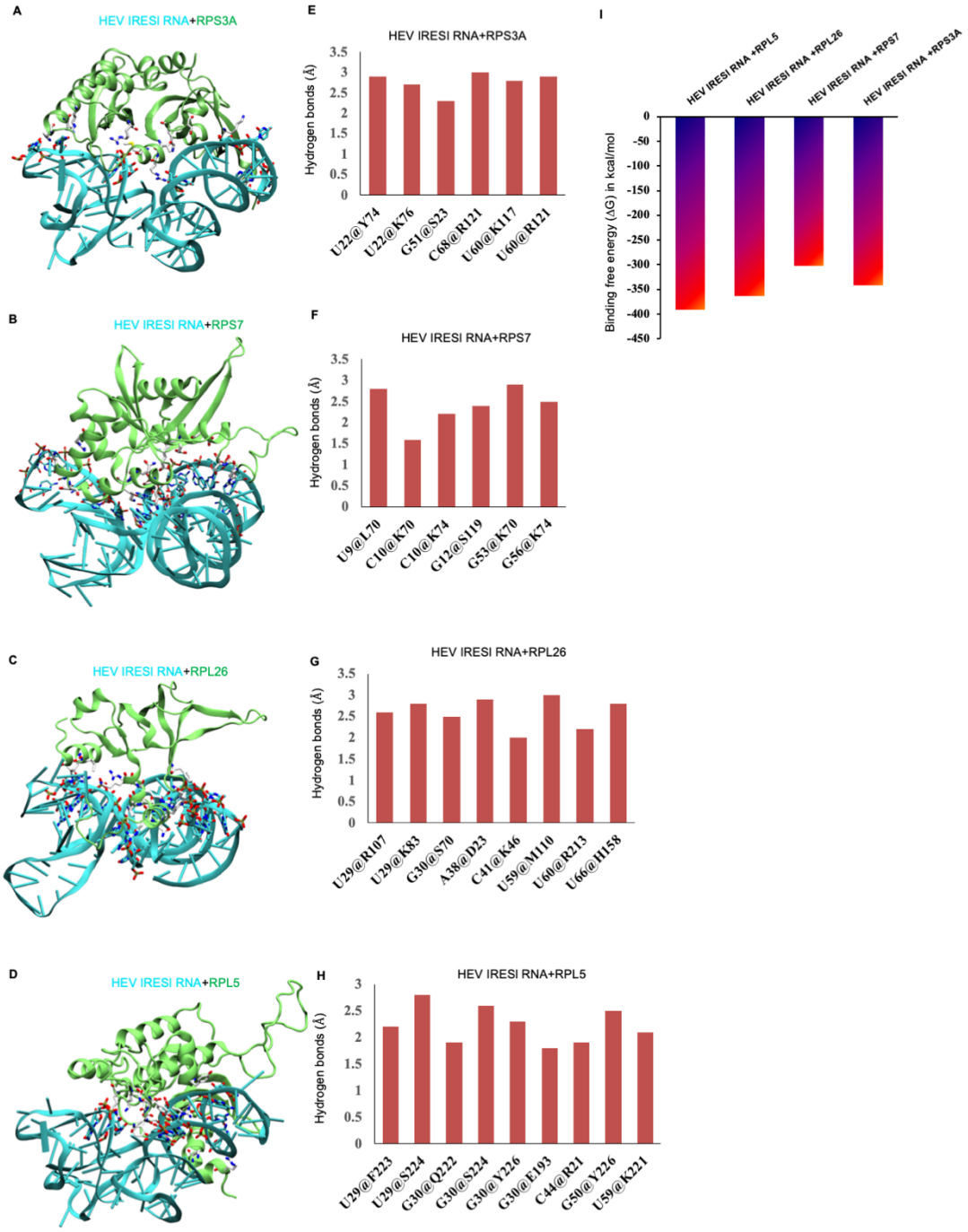
A
HEV IRESI RNA+RPS3A
B
HEV IRESI RNA+RPS7
C
HEV IRESI RNA+RPL26
D
HEV IRESI RNA+RPL5
E
HEV IRESI RNA+RPS3A
Hydrogen bonds (Å)
U22@Y74
U22@K76
G51@S23
C68@R121
U60@K117
U60@R121
F
HEV IRESI RNA+RPS7
Hydrogen bonds (Å)
U9@L70
C10@K70
C10@K74
G12@S119
G53@K70
G56@K74
G
HEV IRESI RNA+RPL26
Hydrogen bonds (Å)
U29@R107
U29@K83
G30@S70
A38@D23
C41@K46
U59@M110
U60@R213
U66@H158
H
HEV IRESI RNA+RPL5
Hydrogen bonds (Å)
U29@F223
U29@S224
G30@Q222
G30@S224
G30@Y226
G30@E193
C44@R21
G50@Y226
U59@K221
I
HEV IRESI RNA +RPL5
HEV IRESI RNA +RPL26
HEV IRESI RNA +RPS7
HEV IRESI RNA +RPS3A
Binding free energy (ΔG) in kcal/mol

369

370 **Figure 5. *In silico* mapping of the interaction between the HEV IRESI RNA and the**
371 **ribosomal proteins.**

372 (A) The interaction between the HEV IRESI and RPS3A is shown in the cartoon and
373 rendered in cyan and lime, respectively. The interacting nucleotides and amino acids are
374 rendered in licorice and colored in atom-wise mode like C: cyan/white, O: red, N: blue
375 and S: yellow. (B) The interaction between the HEV IRESI and RPS7 is shown in the
376 cartoon and rendered in cyan and lime, respectively. The interacting nucleotides and
377 amino acids are rendered as shown in (A). (C) The interaction between the HEV IRESI
378 and RPL26 is shown in the cartoon and rendered in cyan and lime, respectively. The
379 interacting nucleotides and amino acids are rendered as shown in (A). (D) The interaction
380 between the HEV IRESI and RPL5 is shown in the cartoon and rendered in cyan and
381 lime, respectively. The interacting nucleotides and amino acids are rendered as shown in
382 (A). (E-H) The quantitative polar contacts between nucleotide and amino acids are
383 measured for the indicated complexes and shown in bar-graph (Y-axis: hydrogen bond
384 distance, X-axis interacting pair of nucleotides@aminoacids). (I) The binding free energy
385 for the indicated complexes are plotted in the bar graph.

386

387 **RPL5 and DHX9 (RNA helicase A) proteins are essential for the function of the HEV**
388 **IRESI.**

389 In order to further examine the functional significance of host interaction partners of the
390 HEV IRESI, we used siRNA against some of the host factors to deplete them in the Huh7
391 cells, followed by measurement of HEV IRESI activity and g1-HEV replication. 72 hours
392 treatment of Huh7 cells with the siRNAs against RPL5, RPL24, RPL26, RPL41, RPS3A
393 and DHX9 depleted the corresponding proteins (Fig. 6A). Note that in the case of RPS3A
394 siRNA, there was a significant reduction in the GAPDH protein level at 72 hours treatment
395 period (Fig. 6A). Effect of siRNA treatment on viability of the Huh7 cells was measured at
396 72 hours post treatment. RPS3A siRNA treatment led to a significant loss of cell viability
397 (Fig. 6B). Therefore, RPS3A siRNA was excluded from further studies.

398 Next, a bicistronic reporter construct (pRL-FF/Luc dual luciferase construct) was used to
399 simultaneously measure the HEV IRESl activity (by measuring Firefly-Luc activity) and
400 cap-dependent translation activity (by measuring Renilla-Luc activity) in siRNA treated
401 Huh7 cells, as described earlier (27) (Fig. 6C). Among the ribosomal proteins, siRNAs
402 against RPL5 and RPL26 significantly reduced the activity of both Firefly-Luc (measure
403 HEV IRESl activity) and Renilla-Luc (measure cap-dependent translation activity) (Fig.
404 6D, 6E). Lack of RPL 24 and RPL41 did not affect the Firefly-Luc or Renilla-Luc activity
405 (Fig. 6D, 6E). DHX9 siRNA significantly decreased the activity of both Firefly-Luc and
406 Renilla-Luc (Fig. 6D, 6E). Next, g1-HEV expressing Huh7 cells were treated with different
407 siRNAs, followed by measurement of the level of viral sense strand RNA. Lack of RPL5
408 and DHX9 proteins significantly reduced the level of g1-HEV RNA (Fig. 6F). However,
409 lack of RPL24 and RPL26 did not affect g1-HEV RNA level and lack of RPL41 marginally
410 enhanced the level of g1-HEV RNA (Fig. 6F).

411

Figure 6

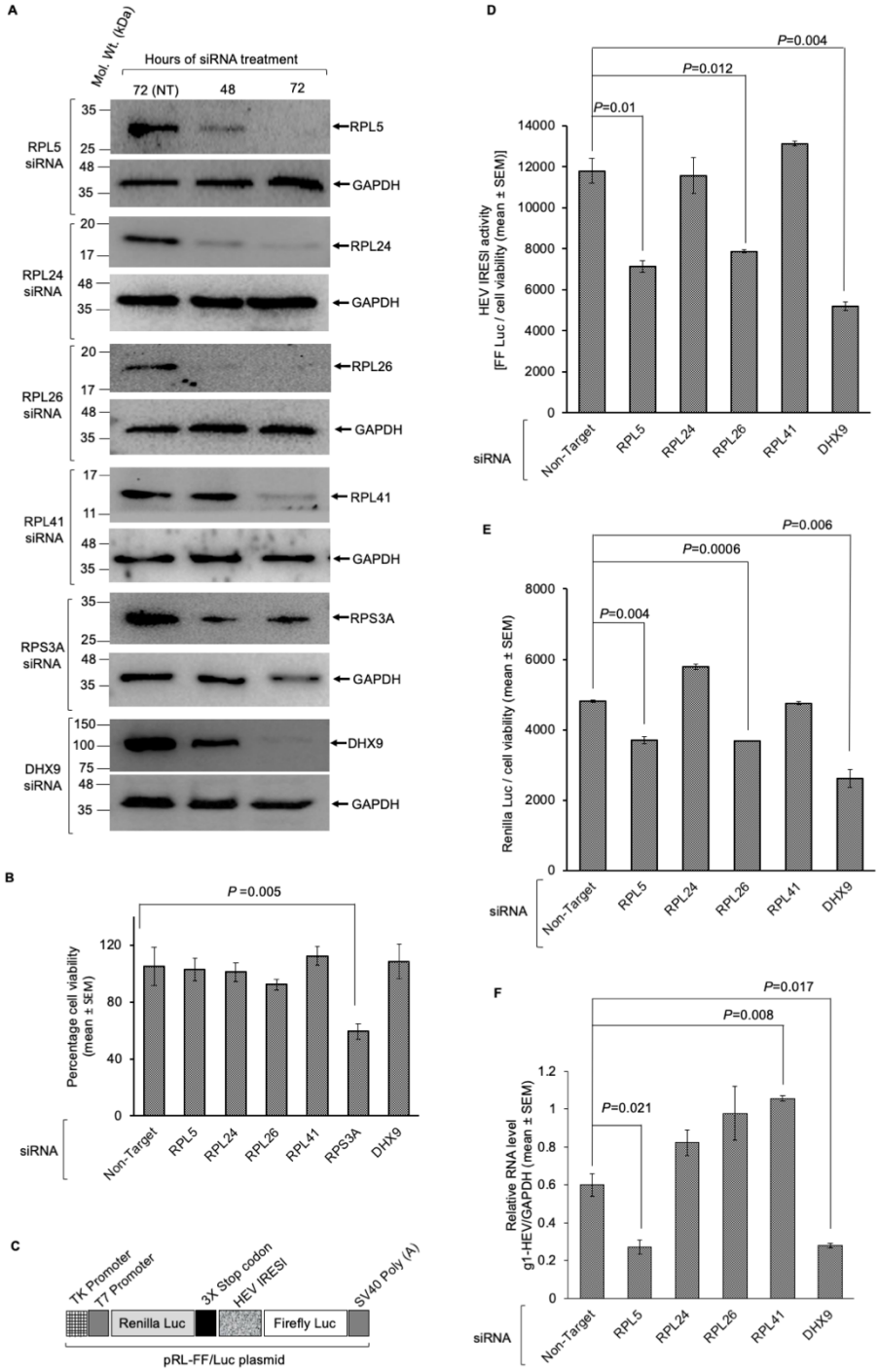
A
Mol. Wt. (kDa)
Hours of siRNA treatment
72 (NT)
48
72
RPL5 siRNA
RPL24 siRNA
RPL26 siRNA
RPL41 siRNA
RPS3A siRNA
DHX9 siRNA
RPL5
RPL24
RPL26
RPL41
RPS3A
DHX9
GAPDH
B
P =0.005
Percentage cell viability (mean ± SEM)
siRNA
Non-Target
RPL5
RPL24
RPL26
RPL41
RPS3A
DHX9
C
TK Promoter
T7 Promoter
3X Stop codon
HEV IRESI
SV40 Poly (A)
Renilla Luc
Firefly Luc
pRL-FF/Luc plasmid
D
P=0.004
P=0.012
P=0.01
HEV IRESI activity [FF Luc / cell viability (mean ± SEM)]
E
P=0.006
P=0.0006
P=0.004
Renilla Luc / cell viability (mean ± SEM)
F
P=0.017
P=0.008
P=0.021
Relative RNA level g1-HEV/GAPDH (mean ± SEM)

412

413 **Figure 6. Essential roles of the ribosomal protein RPL5 and RNA helicase DHX9 in**
414 **mediating the function of the HEV IRESl element.**

415 (A) Western blot analysis of the indicated proteins after 48 and 72 hours treatment with
416 the indicated siRNAs (lanes 2 and 3). Lane 1 shows protein from cells treated for 72 hours
417 with a Non-target siRNA (NT) (B) Percent viability of Huh7 cells treated with the indicated
418 siRNAs for 72 hours. The value for the Non-Target siRNA treated cells was considered
419 to be 100% and other values were calculated relative to that. Values are the mean (±
420 SEM) of triplicate samples (C) Schematic of the pRL-FF/Luc bicistronic reporter plasmid
421 (D) Firefly-Luciferase activity of Huh7 cells transfected with the indicated siRNAs and the
422 pRL-FF/Luc plasmid for 72 hours. The Firefly-Luc values were divided by that of the cell
423 viability and represented as mean (± SEM) of triplicate samples (E) The Renilla-
424 Luciferase activity of the Huh7 cell lysate used in (C). The Renilla-Luc values were divided
425 by that of the cell viability and represented as mean (± SEM) of triplicate samples (F)
426 RTq-PCR measurement of intracellular level of the g1-HEV genomic RNA in the Huh7
427 cells transfected with the indicated siRNAs for 72 hours. Values for the g1-HEV RNA was
428 normalized to that of the GAPDH RNA and represented as mean (± SEM) of triplicate
429 samples.

430

431 **HEV IRESl RNA is associated with the polysomes in translationally active cells.**

432 A ribosomal fractionation assay was performed to verify the localization of the HEV IRESl
433 element in actively translating ribosomes (Fig. 7A). A construct expressing the Firefly-Luc
434 reporter under control of the HEV IRESl in a cap-independent manner (pSuper-HEV
435 IRESl) was used to distinctly identify the presence of the HEV IRESl in the actively
436 translating ribosomes. Note that HEV IRESl RNA transcription is driven by the H1 RNA
437 polymerase III promoter in the pSuper vector. A Renilla-Luc reporter driven by cap-
438 dependent translation was used as a positive control for the assay (pRL-TK). HEK 293T
439 cells were cotransfected with the pSuper-HEV IRESl and the pRL-TK plasmids. 48 hours
440 post transfection, cells were lysed and Firefly, Renilla-Luc activity was measured. As
441 expected, significant activity of both Firefly and Renilla-Luc was observed (Fig. 7B). In

442 order to verify if Firefly-Luc was produced through a cap-independent process, total RNA
443 was isolated from the cotransfected cells, followed by immunoprecipitation of capped
444 RNAs using the anti-$m^7G$ cap antibody, which specifically recognizes the $m^7G$ in the cap
445 structure (37). Level of the Firefly or the Renilla-Luc encoding RNA was quantified by
446 Real-Time PCR. As expected, the Renilla-Luc RNA was detected in the anti-$m^7G$ cap
447 antibody immunoprecipitated sample whereas the Firefly-Luc RNA was not detectable in
448 aliquots of the same sample (Fig. 7C). In contrast, the Firefly-Luc RNA was detected in
449 the unbound fraction only (Fig. 7C).

450 Next, cytoplasmic fractions of HEK 293T cells cotransfected with the pSuper-HEV IRESl
451 and the pRL-TK plasmids were subjected to linear (10-50%) sucrose density gradient
452 centrifugation, followed by measurement of both Firefly and Renilla-Luc RNAs in different
453 fractions. Cells were lysed after treatment with cycloheximide (CHX) or puromycin (Puro),
454 which stalls translating ribosomes or prevents the polysome assembly, respectively
455 (38,39). Ribosome profiles of cycloheximide and puromycin treated cells showed an
456 expected pattern, in agreement with the earlier studies (Fig. S4A, S4B) (39). Total RNA
457 was isolated from aliquots of the alternate fractions from the density gradient samples
458 and resolved by formaldehyde-agarose gel electrophoresis, followed by visualization of
459 28S and 18S RNA by ethidium bromide staining. As expected, 28S and 18S RNA was
460 majorly present in the fractions corresponding to the polysomes in the cycloheximide
461 treated samples (Fig. 7D, left panel), which was significantly reduced in the puromycin
462 treated samples (Fig. 7D, right panel). RT qPCR revealed that in cycloheximide treated
463 cells both Firefly and Renilla-Luc RNA were predominantly detected in the fractions 9
464 onwards, indicating their association with the polysomes (Fig. 7E, left panel). On the other
465 hand, puromycin treatment shifted the detection of Firefly and Renilla-Luc RNA to lighter
466 fractions, fraction 3 onwards (representing 40S, 60S and 80S ribosome subunits),
467 indicating that the HEV IRESl RNA is associated with the polysomes under normal
468 translation condition (Fig. 7E, right panel). Next, aliquots of the density gradient fractions
469 were used for western blot analysis of the different ribosomal proteins, PPIG and DHX9.
470 In cycloheximide treated cells, RPS3A, RPL26, RPS7, RPL5 and RPL24 were
471 predominantly present in the polysomal fractions (Fig. 7F, left panel). Puromycin
472 treatment shifted their distribution towards non polysomal fractions (40S to 60S ribosome)

473 (Fig. 7F, right panels). PPIG and DHX9 were predominately found in the free mRNA or
474 40S-80S ribosome complex-containing fractions, both in cycloheximide and puromycin
475 treated cells (Fig. 7F). PPIG was used as a control to monitor purity of the polysome
476 fractions as it is not known to be present in the polysomes. Note that PPIG is a peptidyl-
477 prolyl isomerase of the cyclophilin family, which catalyze the conversion between *cis* and
478 *trans* isomers of proline (40). Collectively, these findings confirm that the HEV IRESl RNA
479 is complexed with actively translating ribosomes.

**Figure 7**

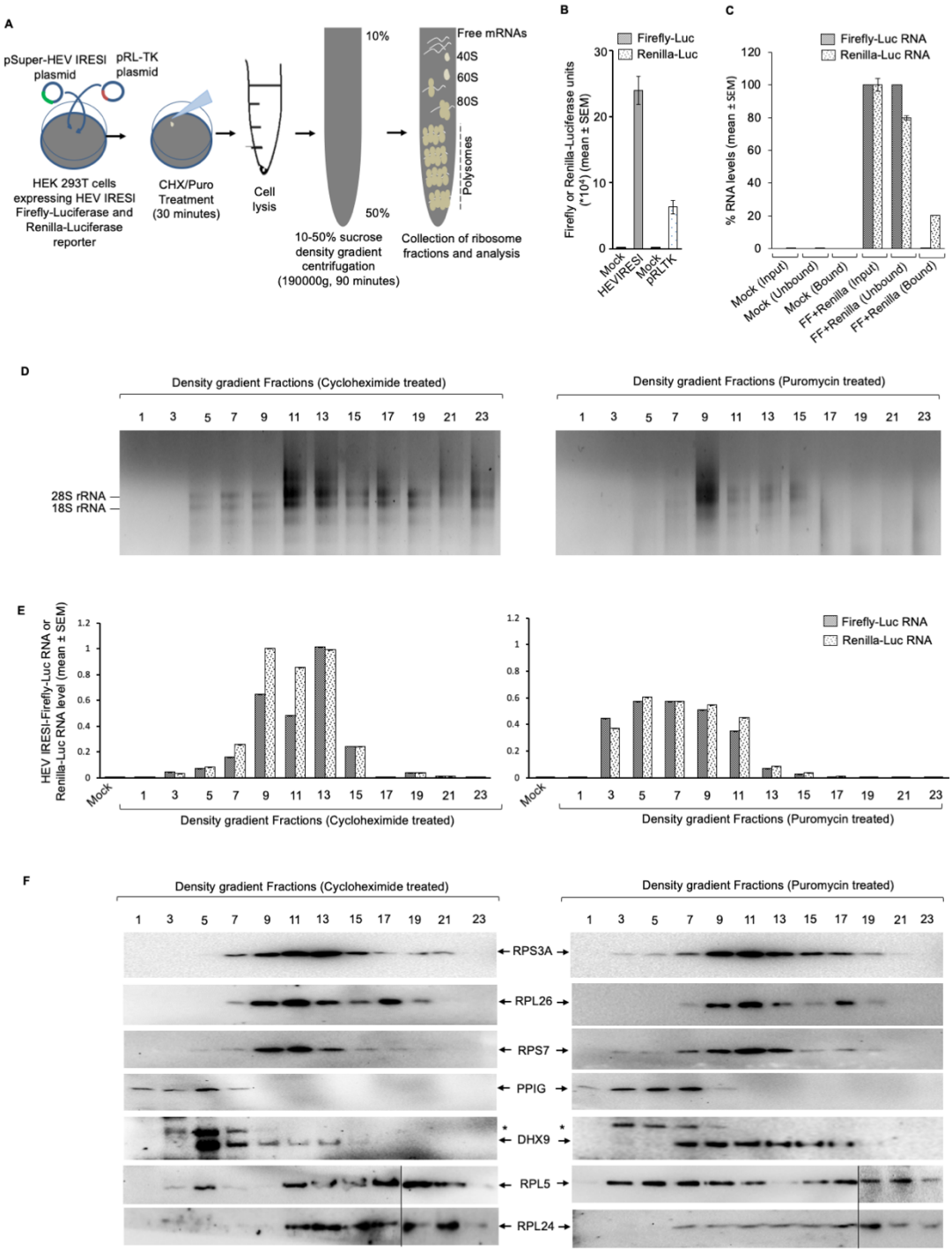
A
pSuper-HEV IRESI plasmid
pRL-TK plasmid
HEK 293T cells expressing HEV IRESI Firefly-Luciferase and Renilla-Luciferase reporter
CHX/Puro Treatment (30 minutes)
Cell lysis
10%
50%
10-50% sucrose density gradient centrifugation (190000g, 90 minutes)
Free mRNAs
40S
60S
80S
Polysomes
Collection of ribosome fractions and analysis
B
Firefly-Luc
Renilla-Luc
Firefly or Renilla-Luciferase units (*10⁴) (mean ± SEM)
Mock
HEV IRESI
Mock
pRLTK
C
Firefly-Luc RNA
Renilla-Luc RNA
% RNA levels (mean ± SEM)
Mock (Input)
Mock (Unbound)
Mock (Bound)
FF+Renilla (Input)
FF+Renilla (Unbound)
FF+Renilla (Bound)
D
Density gradient Fractions (Cycloheximide treated)
Density gradient Fractions (Puromycin treated)
28S rRNA
18S rRNA
E
HEV IRESI-Firefly-Luc RNA or Renilla-Luc RNA level (mean ± SEM)
Firefly-Luc RNA
Renilla-Luc RNA
Mock
Density gradient Fractions (Cycloheximide treated)
Density gradient Fractions (Puromycin treated)
F
Density gradient Fractions (Cycloheximide treated)
Density gradient Fractions (Puromycin treated)
RPS3A
RPL26
RPS7
PPIG
DHX9
RPL5
RPL24

480

481 **Figure 7. The HEV IRESl element associates with actively translating ribosomes.**

482 (A) Schematic of the ribosome fractionation assay. CHX: Cycloheximide, Puro: Puromycin (B)
483 Measurement of the Firefly and the Renilla-Luciferase activities in the Huh7 cells, cotransfected
484 with the pSuper-HEV IRESl and the pRL-TK plasmids. Mock shows pSuper vector transfected
485 Huh7 cells, processed in parallel. Values are represented as mean (± SEM) of triplicate samples
486 (C) RTq-PCR analysis of the Firefly-Luc and the Renilla-Luc RNAs obtained by the RNA-IP assay
487 using anti- $m^7G$-cap antibody. Mock: RNA from the pSuper vector transfected Huh7 cells,
488 FF+Renilla: RNA from the Huh7 cells cotransfected with the pSuper-HEV IRESl and pRL-TK
489 plasmids, Input: amount of RNA used for RNA-IP, Unbound: RNA isolated from supernatant of
490 the IP samples before washing, Bound: RNA isolated from the elution fraction of the IP samples.
491 Values are shown as mean (± SEM) of triplicate samples. (D) Formaldehyde-agarose gel
492 electrophoresis of total RNA isolated from the sucrose density gradient fractions of the Huh7
493 cells, cotransfected with the pSuper-HEV IRESl and pRL-TK plasmids and treated with
494 cycloheximide (left panel) or puromycin (right panel). (E) RTq-PCR analysis of the Firefly-Luc
495 RNA and the Renilla-Luc RNA levels in aliquots of the RNA shown in (D). Values are mean of
496 duplicate samples. (F) Western blot analysis of the level of indicated proteins present in the
497 density gradient fractions, as shown in (D). "*": non-specific band detected by the anti-DHX9
498 antibody.

499

500 Importance of the HEV IRESl RNA-binding translation-related proteins in driving the
501 association of the HEV IRESl RNA with the polysomes was further assessed by a
502 ribosome fractionation assay in Firefly and Renilla-Luc expressing, different siRNA and
503 cycloheximide-treated HEK 293T cells. Fractions 5 and 13 from the density gradient
504 centrifugation samples were analyzed to quantify the levels of Firefly and Renilla-Luc
505 RNAs in the 40S-60S ribosome complex or the polysome complex, respectively.
506 Treatment of cells with siRNAs against RPL5, RPL26 and DHX9 significantly reduced the
507 HEV IRESl RNA association with the polysomes whereas siRNAs against RPL24 and
508 RPL41 did not affect that (Fig. 8A). However, in the case of Renilla-Luc RNA, in addition
509 to RPL5 and RPL26, treatment with RPL24 siRNA also significantly reduced the
510 association of the Renilla-Luc RNA with the polysomes. Further, treatment with DHX9 or
511 RPL41 siRNAs did not affect the association of the Renilla-Luc RNA with the polysomes

512 (Fig. 8B). Next, aliquots of the above samples were analyzed for detection of the RPL5
513 protein (an indicator of polysome-containing fractions). As expected, RPL5 was
514 predominately detected in the polysome-containing fractions (Fig. 8C, Non-Target
515 siRNA). Treatment with RPL5 siRNA significantly reduced its level. Treatment with RPL24
516 and RPL26 siRNAs decreased the level of polysomes whereas RPL41 and DHX9 siRNA
517 treatment did not affect the polysomes (Fig. 8C). These findings confirm the association
518 of the HEV IRESl RNA with actively translating ribosomes and suggest that RPL5 and
519 RPL26 help in HEV IRESl-mediated translation by holding it in the polysomes whereas
520 DHX9 controls HEV IRESl activity independent of its localization to the polysomes.

521

**Figure 8**

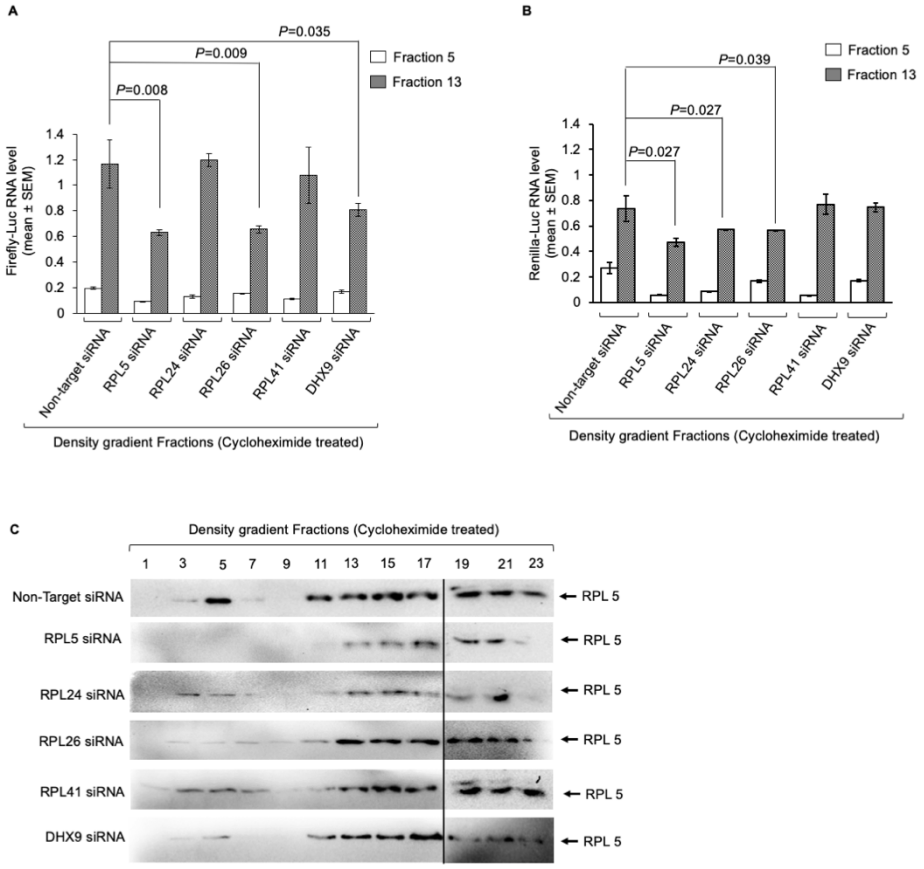


522

523

524 **Figure 8. RPL5, RPL26 and RNA helicase A are important for association of the HEV**
525 **IRESl element with the polysome.**

526 (A) RTq-PCR analysis of the Firefly-Luc RNA level in the density gradient fraction-5 and
527 fraction-13 of the Huh7 cells, transfected with the indicated siRNAs and the pSuper-HEV
528 IRESl and pRL-TK plasmids for 72 hours and treated with Cycloheximide for 30 minutes.
529 Values are mean (± SEM) of triplicate samples. (B) RTq-PCR analysis of the Renilla-Luc
530 RNA level in the density gradient fraction-5 and fraction-13 of the Huh7 cells, transfected
531 with the indicated siRNAs and the pSuper-HEV IRESl and the pRL-TK plasmids for 72
532 hours and treated with Cycloheximide for 30 minutes. Values are mean (± SEM) of
533 triplicate samples. (C) Western blot analysis of the RPL5 protein level in the indicated
534 density gradient fractions of the Huh7 cells, transfected with the indicated siRNAs and the
535 pSuper-HEV IRESl and the pRL-TK plasmids for 72 hours and treated with Cycloheximide
536 for 30 minutes.

537

538 **Discussion**

539 The Hepatitis E virus is a positive strand RNA virus of the family Hepeviridae. The viral
540 genome is capped at the 5'-end followed by a short UTR of 25 nucleotides. The viral non-
541 structural proteins are synthesized from the ORF1 located between 26-5107 nucleotides.
542 Viral capsid protein is produced by the ORF2, located at the 3'-end between 5145-7127
543 nucleotides. A short 3'-UTR of 65 nucleotides is present downstream of the ORF2,
544 followed by a poly-A tail (41). A third ORF is present between the ORF1 and ORF2, which
545 produces ORF3 protein, an accessory protein that associates with the host Tumor
546 susceptibility gene 101 and facilitates release of the progeny virus (42,43,44). The above
547 genome organization is conserved among the 7 genotypes of the HEV. In contrast to
548 zoonotic nature of some HEV genotypes, g1-HEV infection is restricted to the human.
549 The g1-HEV does not replicate efficiently in mammalian cell lines (45). While investigating
550 the cause of poor replication of the g1-HEV in the Huh7 cells, we observed better viral
551 replication upon treatment of cells with ER stress-inducing compounds such as
552 tunicamycin and thapsigargin. Subsequently, we identified a fourth ORF in the viral

553 genome, which produced the ORF4 protein that played a key role in the assembly of the
554 viral replication complex (27). We also observed that ORF4 was synthesized by an
555 internal translation process through an RNA regulatory element. Bicistronic reporter
556 assay and site-directed mutagenesis studies showed that the RNA regulatory element
557 responsible for ORF4 translation acts as an IRES-like (HEV IRESl) element. Sequence
558 analysis of the HEV IRESl indicated its weak homology with the Equine Rhinitis A virus
559 (ERAV) IRES (a type II IRES) (27,46).

560 However, the HEV IRESl element is remarkably smaller in size than other canonical IRES
561 elements and it requires only 87 nucleotides to drive the cap-independent translation of
562 the ORF4 protein in its native context as well as to drive the translation of a heterologous
563 protein such as the Firefly-Luciferase, when inserted into a bicistronic reporter construct.
564 In contrast, function of known IRES elements depend on double the number of
565 nucleotides or more. Smaller size and relatively simple secondary structure of the HEV
566 IRESl element offers the advantage of dissecting out the molecular mechanisms that are
567 crucial for initiation of cap-independent internal translation. Therefore, the current study
568 was undertaken to further substantiate the claim that HEV IRESl element is a bonafide
569 cap-independent internal translation initiation site.

570 Two independent approaches were followed to identify the host interaction partners of the
571 HEV IRESl RNA: RaPID assay and Y3H assay. The RaPID assay identifies stable and
572 transient interactions of all proteins associated with the RNA of interest that includes both
573 direct and indirect interaction partners of the RNA. Several controls were used to
574 avoid/subtract non-specific interaction partners, thus ensuring generation of high
575 confidence mass spectrometry data for downstream studies. For example, good quality
576 of our HEV IRESl RaPID assay-LC-MS-MS data is evident from the fact that comparison
577 of the HEV IRESl-interacting proteins with the SARS-CoV2 5'- and 3'-UTR RNA-
578 interacting proteins (reported by our laboratory using the same technique) identified only
579 RPL7a as the common protein (29). RPL7a is an essential component of the large subunit
580 of ribosome and known to directly bind with RNA through its two distinct RNA binding
581 domains (47). Presence of RPL7a in both the datasets seems to be in agreement with its
582 required function rather than being an experimental artefact.

583 A limitation of the RaPID assay is attributed to its dependence on biotinylation of lysines
584 exposed on the surface of RNA-binding proteins present within 10 nm distance from the
585 BirA ligase. Thus, it is possible to lose some of the RNA binding proteins if they are buried
586 deep inside the complex and inaccessible to BirA ligase for biotinylation. Therefore, a
587 conventional Y3H assay based human liver cDNA library screening was conducted in
588 parallel to identify the interaction partners of the HEV IRESl RNA. Y3H assay offers the
589 advantage of identifying the direct interaction partners of a bait RNA. Y3H assay identified
590 ribosomal proteins (RPL5, RPL26, RPL41, RPS7, RPS15A and RPS3A), a known DNA
591 binding protein (GREBP) and a cyclophilin family protein (PPIG) as interaction partners
592 of the HEV IRESl (48,40). Specificity of the Y3H data was further ensured by assessing
593 the interaction of the eight HEV IRESl RNA-interacting proteins with two well-known IRES
594 sequences such as the FMDV IRES (Type II IRES) and the HCV IRES (Type IV IRES).
595 Distinct patterns of interaction were observed for these RNA sequences, supporting the
596 specificity of the interactions detected in Y3H assay. In order to further confirm the direct
597 interaction between the HEV IRESl RNA and the host proteins, molecular docking
598 analysis was performed for four of the ribosomal proteins, which clearly showed their
599 direct interaction. Docking analysis also demonstrated that the complex between the HEV
600 IRESl and RPL5 was the most stable with respect to the others. Moreover, comparative
601 interaction mapping showed that the interaction of the HEV IRESl element with the
602 ribosomal proteins majorly involved the SL A (nucleotides U9, C10, G12, U22), SL B
603 (nucleotides U29, G30, A38, C41, C44, G50) and the unpaired region between the SL B
604 and SL C (G51, G53, G56, U59, U60, U66, C68) of the former (refer to the HEV IRESl
605 secondary structure in Fig. 1A). In summary, multiple validation steps ensured that the
606 HEV IRESl RNA interaction partners identified in our experiments are of high confidence.

607 Bioinformatics analysis of the 51 HEV IRESl RNA-binding proteins revealed enrichment
608 of proteins involved in the translation process. Note that eight ribosomal proteins and six
609 translation regulatory factors interact with the HEV IRESl RNA, in agreement with its
610 function as an internal translation initiation site**.** Also note that four proteins identified in
611 our study are known to interact with the IRES of other viruses.

612 Silencing of RPL5 significantly inhibited the HEV IRESl activity as well as the g1-HEV
613 replication. RPL5 strongly interacts with the HEV IRESl, weakly interacts with HCV IRES
614 and does not interact with FMDV IRES in Y3H assay. RPL5 showed lowest binding free
615 energy ($\Delta$G) for interaction with the HEV IRESl RNA, *in silico*. RPL5 is also a component
616 of the polysome and lack of RPL5 significantly affected the polysome stability and
617 dissociated both the HEV IRESl and the Renilla-Luc RNAs from the polysome. Hence, it
618 is clear that RPL5 is an essential factor for both cap-dependent and cap-independent
619 translation process. RPL26 showed a pattern similar to RPL5 by inhibiting the HEV IRESl
620 activity and cap-dependent translation. Moreover, the HEV IRESl and the Renilla-Luc
621 RNA association with the polysome was significantly reduced upon treatment of cells with
622 the siRNA against RPL26. However, RPL26 differs from RPL5 in the following
623 parameters: it binds moderately with the HEV IRESl RNA both in Y3H assay and *in silico*
624 analysis and lack of RPL 26 marginally affects the polysome stability. Earlier studies have
625 shown that lack of RPL26 does not affect cap-dependent translation in *Saccharomyces*
626 *cerevisiae* and RPL26 is a known ITAF, which has been shown to control DNA damage
627 induced cap-independent translation of the p53 mRNA (49,50,51). Taken together, these
628 data suggest a role of RPL26 in mediating efficient function of the HEV IRESl though it is
629 not an essential factor. Ablation of both RPL5 and RPL26 may show a more profound
630 effect on the HEV IRESl activity. Silencing of RPL24 and RPL41 did not inhibit either the
631 HEV IRESl activity or the Renilla-Luc activity. Lack of RPL24 reduced the stability of the
632 polysomes, which is in agreement with earlier reports (52). However, lack of RPL24 did
633 not affect the HEV IRESl RNA association with the polysomes although it reduced the
634 association of the Renilla-Luc RNA with the polysomes, indicating its importance in cap-
635 dependent translation. Lack of RPL41 did not affect the polysome stability or HEV IRESl
636 and Renilla RNA association with the polysomes. Interestingly, lack of RPL41 significantly
637 increased the g1-HEV replication, possibly due to extra-translational function of RPL41.
638 Note that RPL41 knockdown has been shown to arrest the cell-cycle in the G2/M phase
639 and it acts by stabilizing the microtubule (53). Our earlier study has shown that HEV
640 replication is significantly high in the G2/M phase of the cell-cycle (54).

641 Apart from the ribosomal proteins, DHX9/RNA helicase A (RHA), HNRNPA2/B1,
642 YTHDF2, EEF2 and LARP4 were also identified as interaction partners of the HEV IRESl

643 RNA. RHA is known to associate with the IRES of FMDV and HCV and acts as an ITAF.
644 It also promotes translation from the IRES of retroviral RNA and jun D mRNA and
645 regulates the replication of several RNA viruses, including the porcine reproductive and
646 respiratory syndrome virus, bovine viral diarrhea virus, classical swine fever virus and
647 dengue virus (55,56,57,58). It binds to the 3'-UTR of HEV, however significance of the
648 interaction is not known (59). RHA is a member of the DEx H-box family of superfamily II
649 (SF2) helicases, which unwind duplex RNA possessing a 3'-single stranded RNA tail by
650 hydrolyzing the nucleoside triphosphates (60,61). In our experiments, lack of RHA
651 significantly reduced both the HEV IRESl and the Renilla-Luc activities as well as reduced
652 the g1-HEV replication. It was found to be associated with the 40S-80S ribosomes and
653 polysomes, however, its absence did not affect the polysome stability. Lack of RHA
654 resulted in reduced recruitment of the HEV IRESl RNA to the polysomes, however,
655 Renilla-Luc RNA association with the polysomes was not affected. Thus, RHA seems to
656 be involved in controlling the function of the HEV IRESl as well as g1-HEV replication.
657 HNRNPA2B1 is reported to be involved in mRNA processing. It has been shown to bind
658 to the 3'-UTR of CDK6 and recruit RHA, leading to miRNA mediated silencing of CDK6
659 (62). An earlier study has shown that HNRNPA2B1 binds to the genomic and sub genomic
660 promoters of HEV and plays an essential role in the g1-HEV replication. Further,
661 intracellular localization of HNRNPA2B1 is altered in the HEV infected cells (63). YTHDF2
662 is known to accelerate mRNA decay by targeting the mRNAs to cytoplasmic processing
663 bodies (P-bodies) and by recruiting the CCR4-NOT deadenylase complex (64,65). EEF2
664 (eukaryotic elongation factor 2) is a GTP binding translation elongation factor, which plays
665 an essential role in translation by promoting GTP dependent translocation of the ribosome
666 (66). LARP4 binds to the poly-A tract of mRNA, associates with the 40S ribosomal subunit
667 as well as polysomes and plays a role in translation regulation by preventing
668 deadenylation at poly-A tail (67,68,69). Presence of these factors in the HEV IRESl RNA-
669 associated protein complex suggests their potential role(s) in regulating the HEV IRESl-
670 mediated translation. Further studies are warranted to clarify their mode of action.

671 An important aspect of the HEV IRESl function pertains to upregulation of its activity by
672 the ER stress inducing agents in the g1-HEV infected cells (27). The RaPID assay
673 identified four proteins involved in the ER stress response pathway such as the heat

674 shock protein 105 kDa (HSP 105), the luminal ER protein of 29 kDa (ERp29), γ-taxilin and
675 Pumilio homolog 1 (PUM1) as interaction partners of the HEV IRESl. HSP 105 is known
676 to regulate the ER stress induced caspase-3 activation (70). ERP29 is induced by the ER
677 stress. It is ubiquitously expressed and implicated in the biosynthesis and trafficking of
678 many proteins (71). γ-taxilin belongs to the syntaxin-binding protein family, it interacts with
679 ATF4 and regulates the ER stress response (72). PUM1 is known to be phosphorylated
680 by the IRE1 kinase under conditions of ER stress, it binds spliced XBP1 RNA and
681 prevents its degradation (73). Upon ER stress, interaction between PUM1 and HEV IRESl
682 might be protecting the later from degradation by the regulated IRE1-dependent decay
683 (RIDD) pathway.

684 In conclusion, we have identified 51 host proteins, which associate with the HEV IRESl
685 RNA in mammalian cells. Four of the identified proteins have been reported to associate
686 with known IRES elements of viral and cellular origin and two of the identified proteins
687 are known ITAFs. Several ribosomal proteins, translation regulatory factors, components
688 of the tRNA synthetase complex were found to be associated with the HEV IRESl RNA.
689 Taken together, above data unequivocally demonstrate that the HEV IRESl is a bonafide
690 internal ribosome entry site capable of driving cap-independent translation. These
691 findings significantly advance our understanding of the molecular mechanisms that
692 control the synthesis of the ORF4 protein in the g1-HEV infected cells. Moreover,
693 considering the small size and simplicity of the secondary structure of the HEV IRESl
694 element compared to other well-known IRES elements, it is a useful tool for recombinant
695 protein expression as well as for investigating the molecular details of the cap-
696 independent IRES-mediated translation process.

697

698 **Materials and Methods**

699 **Plasmids and reagents**

700 The RNA motif plasmid cloning backbone [(pRMB) (Addgene plasmid # 107253;
701 http://n2t.net/addgene:107253; RRID: Addgene_107253)] and the BASU RaPID plasmid

702 (Addgene plasmid # 107250; http://n2t.net/addgene:107250; RRID:Addgene_107250)
703 were gifted by Prof. Paul A. Khavari (School of Medicine, Stanford University, Clifornia ,
704 USA) and reported earlier (29). To clone the HEV IRESl in the pRMB vector, 2701 to 2787
705 nucleotides of the g1-HEV genome (Genbank ID: AF444002.1) was PCR amplified from
706 the pSK HEV2 plasmid (27) with the following primers: IRESl87 BASU CBB FP (5'
707 GCTTGGTGCCGATCGGTCCC 3') and IRESl87 BASU CBB RP
708 (5'AGCTCATCTGGCAGCAAGCTCAG 3') and ligated with the pRMB vector backbone
709 generated by BSMB1 restriction enzyme digestion, followed by blunting. For hybrid RNA
710 generation for Y3H assay, HEV IRESl, FMDV IRES and HCV IRES sequences were PCR
711 amplified from the pSKHEV2 plasmid, pVitro2-neo-mcs plasmid (InvivoGen, San Diego,
712 USA) and S52/SG-Feo(AI) replicon [gifted by Prof. Charles M. Rice, (74)], respectively,
713 using the following primers: HEV IRESl FP: (5'
714 ACTATCTCGAGGGTGCCGATCGGTCCC 3'), HEV IRESl RP: (5'
715 ACTATCCATGGCATCTGGCAGCAAGCTCAG 3'); FMDV IRES FP: (5'
716 ACTATCTCGAGAGCAGGTTTCCCCAATGACACA 3'), FMDV IRES RP: (5'
717 ACTATCCATGGAAAGGAAAGGTGCCGACCTCCG 3'); HCV IRES FP: (5'
718 ACTATCTCGAGACCTGCCTCTTACGAGGC 3') and HCV IRES RP: (5'
719 ACTATCCATGGTTCTTTGAGGTTTAGGAAGTGTGCT 3'). PCR products were digested
720 with the Xho1 restriction enzyme and ligated with the XhoI and SmaI digested p3HR2
721 vector backbone. To clone the negative sense HEV IRESl (HEVIRESl$^{-}$) fragment in the
722 p3HR2 vector, 87 nucleotides of IRESl sequence was PCR amplified from the pSK HEV
723 plasmid using HEV IRESl FP and HEV IRESl RP primers and ligated with the SmaI
724 digested p3HR2 vector. To clone the HEV IRESl sequence in the pSuper vector,
725 pRLFF/Luc87 and pSuper plasmids were restriction digested with the BamHI and KpnI
726 enzymes, respectively, followed by treatment with Klenow (endfilled by Klenow) and
727 digestion of both plasmids with XhoI and ligation. All clones were confirmed by DNA
728 sequencing. All plasmids are available upon request.

729 Human liver cDNA library was obtained from Clontech (California, USA). Dual Luciferase
730 reporter assay kit and CellTiter96 Aqueous one solution cell proliferation assay kits were
731 from Promega (Madison, USA). Non-targeting siRNA (Catalog no.D-001810-10-20),

732 Human RPL5 (6125) siRNA (Catalog no. L-013611-00-0005), Human RPL26 (6154)
733 siRNA (Catalog no. L-011132-01-0005), Human RPL24 (6152) siRNA (Catalog no. L-
734 011144-02-0005), Human RPL41 (6171) siRNA (Catalog no. L-011160-01-0005), Human
735 RPS3A (6188) siRNA (Catalog no. L-013607-00-0005) Human DHX9 (1660) siRNA
736 (Catalog no. L-009950-00-0005) were from Ge Healthcare Dharmacon (Colorado, USA).
737 Antibodies against RPL5 (Catalog no. A303-933A) and RPL26 (Catalog no. A300-686A)
738 were from Bethyl laboratories (Texas, USA). Anti-RPL24 (Catalog No. ITT09128), anti-
739 RPL41 (Catalog No.ITT09136) and anti-DHX9 (Catalog No. ITT12266) antibodies were
740 from Geno Technology Inc. (St Louis, USA); anti-RPS3A (catalog No. STJ28158), anti-
741 RPS7 (catalog No.STJ28814) and anti-PPIG (catalog No. STJ191133) antibodies were
742 from St. John's laboratory (London, UK). Anti-GAPDH (catalog no. sc-25778) antibody
743 was from Santa Cruz Biotechnology (Texas, USA). Goat anti-rabbit IgG-HRP (Cat No.
744 4030-05) was from Southern Biotech (Alabama, USA). 3-Amino 1, 2, 4 triazole (3-AT),
745 Ortho-Nitrophenyl-β-galactoside (ONPG), Cycloheximide and Puromycin was from
746 Sigma (Missouri, USA). Cycloheximide and puromycin were used at a working
747 concentration of 100µg/ml and 0.5µg/ml, respectively.

748 **Mammalian cell-culture, transfection, *in vitro* transcription and cell viability assay**

749 HEK 293T cells were obtained from ATCC (Virginia, USA). Huh7 cells were as described
750 previously (27). Cells were maintained in Dulbecco's modified Eagle medium (DMEM)
751 containing 10% Fetal Bovine Serum (FBS), 50 I.U./mL Penicillin and Streptomycin at
752 $37^0$C in a 5% $CO_2$ incubator. Cells were maintained in antibiotic free medium before
753 starting the experiments. For plasmid transfection, cells were seeded at 70-80%
754 confluency in DMEM + 10% FBS and incubated overnight at $37^0$C in a 5% $CO_2$ incubator.
755 Next day, cells were transfected with the desired plasmids using Lipofectamine 2000
756 transfection reagent (Thermo Scientific, Massachusetts, USA), at 1:1 ratio, following
757 manufacturer's instruction. 6-8 hours post-transfection, culture medium was replaced with
758 fresh DMEM+10% FBS.

759 For experiments involving siRNA mediated gene silencing, cells were seeded at 70-80%
760 confluency on 12 well TC dishes and incubated overnight at $37^0$C with 5% CO2. Next

761 day, 25nmol siRNA was transfected into each well using 0.35μl Dharmafect transfection
762 reagent, following manufacturer's instruction (GE Healthcare Dharmacon Inc., Colorado,
763 USA). 12 hours post-transfection, culture medium was replaced with fresh medium
764 (DMEM + 10% FBS) and cells were maintained at $37^0$C in a 5% $CO_2$ incubator.

765 The HEV genomic RNA was *in vitro* synthesized as capped RNA, using mMessage
766 mMachine kit (Thermo Scientific, Massachusetts, USA), as described (27). Size and
767 integrity of the *in vitro* synthesized RNA was monitored by formaldehyde agarose gel
768 electrophoresis. *In vitro* synthesized RNA was transfected using Lipofectamine 2000
769 transfection reagent, at 1:1 ratio, following manufacturer's instruction (Thermo Scientific,
770 Massachusetts, USA). 6-8 hours post-transfection, the culture medium was replaced with
771 fresh medium (DMEM+10% FBS) and maintained until further manipulation.

772 Cell viability was measured using a commercially available kit [CellTiter 96 Aqueous One
773 Solution Cell Proliferation Assay (Promega, Madison, USA)], which utilizes Tetrazolium
774 salt based colorimetric assay. Details are as described (27).

775 **Yeast three Hybrid (Y3H) Assay and screening of the human liver cDNA library**

776 A GAL4 based Y3H assay system, gifted by Prof. Marvin Wickens (University of
777 Wisconsin, Madison, USA) was used to determine the RNA-protein interactions and
778 identification of the HEV IRESl RNA-binding proteins by screening of the human liver
779 cDNA library using the YBZ1 Yeast strain (30 ).

780 The YBZ1 competent cells were prepared following Lithium Acetate method, as described
781 (75). To examine self-activation by the p3HR2-HEV IRESl, 2μg each of the p3HR2-HEV
782 IRESl and pACT2 plasmids or p3HR2 and pACT2 plasmids were cotransformed into the
783 YBZ1 competent cells and plated on $LU^-$ media, as described (75). After 3 days of
784 incubation in a humidified incubator at $30^0$C, 8 random colonies were replica plated onto
785 $LUH^-$ as well as 3-AT (0.1-1 mM) supplemented $LUH^-$ plates, followed by 4 days
786 incubation at $30^0$C in a humidified incubator. Colonies were monitored on the $4^{th}$ day. The
787 p3HR2-HEV IRESl-containing colonies showed very little/no growth on the $LUH^-$ and $LUH^-$
788 +3-AT media (Figure S2).

789 Next, 2µg of the p3HR2-HEV IRESl plasmid DNA was transformed into the YBZ1
790 competent cells and plated on the $U^-$ media. After 3 days of incubation at $30^0$C, a single
791 colony was inoculated in the $U^-$ media and grown at $30^0$C to prepare the primary culture
792 (YBZ1-p3HR2-HEV IRESl) and subsequently, the secondary culture. Aliquots of the
793 culture were used for RNA isolation and verification of the HEV-IRESl RNA expression
794 by RT-PCR. Next, the secondary culture grown from the primary culture was used for
795 preparation of competent cells of the YBZ1-p3HR2-HEV IRESl.

796 The human liver Matchmaker cDNA library was procured in the *E.coli BNN132* strain with
797 a titer of $\geq 10^8$ cfu/ml. The cDNA library contained $3.5*10^6$ independent clones, with ~93%
798 colonies containing the cDNA insert. The cDNA library was amplified and a stock titer of
799 $\geq 10^7$ cfu/ml was prepared and stored at $-80^0$C until further use, following the
800 manufacturer's instruction. Plasmid DNA was isolated from the retitered stock and used
801 for transformation into the YBZ1-p3HR2-HEV IRESl competent cells (YBZ1 strain
802 containing the p3HR2-HEV IRESl plasmid). A pilot transformation was performed to
803 estimate the efficiency of the cDNA library and optimize the ideal quantity of DNA required
804 for screening, following the instructions of the manufacturer. Approximately, $4*10^6$
805 independent library clones were screened on the $LUH^-$ + 0.5mM 3-AT media-containing
806 plates (0.5mM 3-AT was added to enhance the stringency of the screening), leading to
807 growth of 395 colonies. Subsequent replica plating of those 395 colonies on $LUH^-$ plates
808 containing an increasing concentration of 3-AT (2mM, 5mM, 10mM and 20mM) showed
809 that all colonies could grow on 10mM 3-AT or more. These colonies were inoculated in 5
810 ml $LU^-$ media and incubated overnight at 200 RPM, $30^0$C, in an incubator-shaker. Next
811 day, cells were harvested by centrifugation at 7000×g, $4^0$C, 10 minutes. Plasmid DNA
812 was isolated using the Qiaprep miniprep kit (Qiagen, Hilden, Germany). Briefly, cell pellet
813 was resuspended in the buffer P1 (supplied in the kit), followed by 6 cycles of freeze-thaw
814 in liquid nitrogen and ambient temperature, respectively. Next, the buffer P2 was added,
815 samples were mixed thoroughly and incubated for 5 minutes at ambient temp. Next, buffer
816 N3 was added, samples were mixed thoroughly and centrifuged at 18000×g, $4^0$C, 10
817 minutes. Supernatant was loaded onto the kit-supplied columns and plasmid DNA was
818 eluted after a series of washing, as per the instruction of the manufacturer. Plasmid DNA

819 isolated from the YBZ1 transformants were transformed into the *E.coli Top*$_{10}$ strain and
820 colonies were grown on the LB agar media containing ampicillin (100 µg/ml). Presence
821 of the pACT2 plasmid with a cDNA insert sequence in the *E.coli* transformants was
822 verified by a colony PCR using the following primers: pACT2 AD-LT seq FP: (5' ATT
823 CGATGATGAAGATACCCCA 3') and pACT2 AD-LT seq RP: (5'
824 GTGAACTTGCGGGGTTTTTCAGTATCTACGA 3'). 285 colonies were positive in the
825 PCR, indicating that they contained a library clone with a cDNA insert. Plasmid DNA was
826 isolated from these colonies and digested with HindIII, XhoI and EcoRI restriction
827 enzymes to sort them into different categories based on their restriction patterns. 75
828 clones were found to contain unique cDNA insert. The insert and its flanking region was
829 sequenced using the following primer: pACT2 AD LT SEQ Primer:
830 TGGTGGGGTATCTTCATCATCGAATAG. Analysis of the sequencing data identified 8
831 unique protein coding gene sequences in frame with the GAL4 AD. These clones were
832 cotransformed along with the p3HR2-HEV IRESl plasmid into the YBZ1 competent cells
833 with appropriate controls to ensure that the interaction is reproducible and there is no self-
834 activation by the prey protein. Liquid β-galactosidase assay of the colonies were done as
835 described earlier (75).

836 **RaPID assay**

837 The RaPID assay was done as described, following similar conditions (29). To identify
838 the HEV IRESl-interacting host proteins, HEK 293T cells were co-transfected with the
839 pRMB HEV IRESl and BASU plasmids (in 6:1 ratio) using lipofectamine 2000 (1:1 ratio).
840 42 hours post-transfection, 200µM biotin supplemented media (DMEM+10%FBS) was
841 added to the cells and maintained for 18 hours.

842 *Cell lysate preparation:* Cells were washed thrice with ice-cold PBS and lysed in prechilled
843 radio-immunoprecipitation (RIPA) buffer (150 mM NaCl, 1% NP-40, 0.5% sodium
844 deoxycholate, 0.1% SDS, 50mM Tris, pH 8.0), supplemented with protease and
845 phosphatase inhibitor cocktail. The lysate was centrifuged at 14000×g for 40 min and a
846 Macrosep advanced filter (3000 Da MW cutoff, 20 ml; catalogue no. 89131-974; VWR,
847 USA) was used to remove the free biotin. Clarified supernatant was precipitated in

848 acetone, first at -20°C for 10 minutes and then at -80°C for 20 minutes. Protein precipitate
849 was solubilized in 8M urea and Bicinchoninic (BCA) protein assay kit (Thermo Fisher
850 Scientific, MA, USA) was used to determine the protein concentrations of each sample.

851 *Digestion and peptide preparation:* 10mg protein for each sample was treated with 10mM
852 DTT (Dithiothreitol), for 30 min at $56^0$C and alkylated with 20mM iodoacetamide (IAA) at
853 room temperature for 1 hour in dark. Trypsin (catalog no.T1426; Thermo Fisher Scientific,
854 MA, USA) was added to the samples at a 1: 20 (wt/wt) ratio and incubated at $37^0$C for 24
855 hours. Next, 1% formic acid was added to the samples and desalting of the peptides was
856 done using a Sep-Pak C18 cartridge (catalog no. WAR020515; Waters, MA, USA)
857 followed by lyophilization in a SpeedVac. Lyophilized peptides were solubilized in 1ml
858 PBS and incubated with 150µl pre-washed streptavidin agarose beads (catalog no.
859 20361; Thermo Fisher Scientific, MA, USA) for 2 hours at ambient temperature. The
860 beads were washed in PBS, followed by washing in wash buffer (5% acetonitrile in PBS)
861 and finally with ultrapure water. Excess liquid was completely removed from beads, and
862 biotinylated peptides were eluted by adding 0.3 ml of a solution containing 0.1% formic
863 acid and 80% acetonitrile in water by boiling at 95°C for 5 min. A total of 10 elutions were
864 collected and dried together in a SpeedVac. Enriched peptides were desalted with C18
865 tips (Thermo Fisher Scientific, MA, USA), and reconstituted with solvent A (2%, v/v,
866 acetonitrile, 0.1% v/v, formic acid in water) for LC-MS/MS analysis.

867 *LC-MS/MS acquisition:* A Sciex $5600^+$ triple time of flight (TOF) mass spectrometer was
868 used for LC-MS/MS analysis. It was coupled with a chromXP reversed-phase 3-µm $C_{18}$-
869 CL trap column (350 µm by 0.5 mm, 120 Å; Eksigent; AB Sciex, MA, USA) and a
870 nanoViper $C_{18}$ separation column (75 µm by 250 mm, 3 µm, 100 Å; Acclaim PepMap;
871 Thermo Fisher Scientific, MA, USA) in an Eksigent nanoLC (ultra 2D plus) system. A
872 binary mobile solvent system was applied, with the following composition: solvent C, 2%
873 (v/v) acetonitrile, 0.1% (v/v) formic acid in water; solvent B, 98% (v/v) acetonitrile, 0.1%
874 (v/v) formic acid. To separate the peptides, a 60 minutes gradient was run with a total run
875 time of 90 minutes at a flow rate of 200 nl/minute and MS data was acquired in information
876 dependent-acquisition (IDA) with high sensitivity mode. Each cycle was run for 2.3
877 seconds with 250- and 100-ms acquisition times for MS1 (*m/z* 350 to 1,250 Da) and

878 MS/MS (100 to 1,800 *m/z*) scans, respectively. Every experimental condition was run in
879 quadruplets.

880 *Protein identification and quantification:* All raw files (.wiff) were searched in proteinPilot
881 software (version4.5; Sciex) with Mascot algorithm for protein identification and
882 semiquantitation against Swiss-Prot_57.15 database (20,266 sequences after application
883 of *Homo sapiens* taxonomy filter). Following parameters were applied to search
884 biotinylated peptides: (a) Trypsin as a proteolytic enzyme with maximum of two missed
885 cleavages allowed. ; (b) Allowed tolerance limit for peptide mass error was 20ppm;(c)
886 Mass error tolerance for fragments was taken up to 0.20 Da; (d) Carbamido-methylation
887 of cysteine (+ 57.02146 Da), oxidation of methionine (+15.99491 Da), deamination of NQ
888 (+ 0.98416), and biotinylation of lysine (+ 226.07759 Da) were taken as variable
889 modifications. Pearson correlation plot of peptide intensity was used to monitor the quality
890 of data between each run and replicates.

891 *Data analysis:* A protein was considered to be identified if it corresponds to one or more
892 biotinylated peptide, with PEP (posterior error probability) score ≥ the median value in the
893 Gaussian smoothing curve of each sample. Note that PEP score refers to the probability
894 that the observed peptide spectrum matches are incorrect. A web-based tool,
895 Bioinformatics and Evolutionary Genomics (http://bioinformatics.psb.ugent.be/
896 webtools/Venn/) was used to identify host proteins that are specific to HEV IRESI RNA
897 and formation of Venn diagram. Data set with a minimum of 1 unique peptide and a "prot
898 score" of 30 or more was considered in the final list of host proteins for further studies
899 (Table1). "Prot Score" refers to the overall protein score generated by Mascot,
900 considering all the observed mass spectrums, which match amino acid sequences of a
901 certain protein.

902 *Data availability:* The mass spectrometry proteomics data have been deposited to the
903 ProteomeXchange Consortium via the PRIDE partner repository with the dataset identifier
904 PXD031009.

905 **Bioinformatics analysis**

906 RNA secondary structures were analyzed using the Mfold program
907 (http://www.unafold.org/mfold/applications/rna-folding-form.php), based on a minimum
908 free energy calculation at $25^0$C (76). The host-virus RPPI data set was visualized using
909 Cytoscape (version 3.1.0). NetworkAnalyzer plug-in in Cytoscape was used to compute
910 the topological parameters and centrality measures of the network. Gene ontology (GO)
911 and Reactome pathway analysis were performed using the Gene Set Enrichment
912 (https://www.gseamsigdb.org/gsea/index.jsp) and Enrichr
913 (https://maayanlab.cloud/Enrichr) (77) tools.

914 ***In silico* analysis of the RNA-protein interactions**

915 The protein structures of the four targets RPS3A, RPS7, RPL5, RPL26 are not reported,
916 therefore, their sequences were retrieved from the "uniport" by using their id numbers
917 P61247, P62081, P46777, and P61254, respectively. Furthermore, the i-tasser module
918 was used to build their 3D structures. Based on their c_score, the best model was
919 selected and evaluated through Ramachandran plots. Furthermore, the energy
920 minimization of each protein was carried out using AMBER tool. The 3dRNA tool is used
921 to generate the 3D of RNA sequence. For Protein-RNA docking, the HDOCK was used
922 with the standard cut-offs. In each docking the top complex was picked for further
923 analysis. The energy minimized complex structures were used for their quantitative and
924 thermodynamic analysis.

925 **Luciferase reporter assay, Western blot analysis, RNA isolation and quantitative**
926 **real time PCR (RTq-PCR)**

927 To perform the dual luciferase reporter assay, the HEK 293T cells were seeded at 70%
928 confluency and next day, 25nM siRNA were transfected in respective wells using 0.35µl
929 of DharmaFECT (GE Healthcare Dharmacon Inc. Co, USA) transfection reagent as per
930 manufacturer's instructions. 12 hours post transfection of siRNA, media was changed
931 followed by transfection of the dual luciferase reporter plasmids (pRLFF/luc87, 1µg/well)
932 using lipofectamine 2000 at 1:1 (wt/v) ratio. 8 hours later, media was changed and cells
933 were incubated for 48 hours. Cells were washed with ice cold PBS and used for luciferase
934 assay using the dual glow Luciferase assay kit, following manufacturer's protocol

935 (Promega, Wisconsin, USA). The Firefly-Luc values were divided by that of the Renilla-
936 Luc or divided by the percentage cell-viability, as specified in the results and graphs were
937 plotted in GraphPad prism or Microsoft Excel. Values are mean (± SEM) of three
938 independent experiments done in triplicates. Western blot was done as described (27).
939 Total cellular RNA was isolated using the TRI reagent (MRC Inc., Cincinnati, USA) as per
940 manufacturer's protocol. cDNA was synthesized using random hexamers and a
941 commercial cDNA synthesis KIT, following manufacturer's protocol (Firescript cDNA
942 synthesis kit, Solis BioDyne, Tartu, Estonia). RTq-PCR was done by SYBR green
943 detection method using a commercially available kit (5X HOT Firepol Evagreen QPCR
944 Mix Plus, Solis BioDyne, Tartu, Estonia). Following primers were used to detect the levels
945 of g1-HEV RNA, HEV IRESl RNA and Renilla-Luc RNA: g1-HEV FP: (5'
946 CGGCCCAGTCTATGTCTCTG 3'), g1-HEV RP: (TAGTTCCTGCCTCCCAAAAG 3');
947 HEV IRESl FP (5' TATACTCGAGGGTGCCGATCGGTCCC 3'), HEV IRESl RP (5'
948 TATACCATGGCATCTGGCAGCAAGCTCAG 3'); R-Luc FP (5'
949 CTTCTTATTTATGGCGACATGTT 3') and R-Luc RP (5' GCCTGATTTGCCCATACC
950 AATA 3').

951 **Ribosome fractionation assay**

952 Ribosome fractionation was done as described (38,39). HEK 293T cells were seeded at
953 70% confluency in 100 mm dishes and transfected with the pSuper-HEV IRESl and pRL-
954 TK plasmid DNA (10µg/dish) using lipofectamine 2000 (1:1 ratio). 48 hours post-
955 transfection, 100 µg/ml of cycloheximide (CHX) or 0.5µg/ml of puromycin (Puro) was
956 added to the culture medium and incubation was continued for 30 minutes at $37^0$C, with
957 5% $CO_2$. Next, cells were washed three times with ice cold PBS (containing 100 µg/ml
958 CHX, in case of CHX treatment) followed by trypsinization and centrifugation for 5 minutes
959 at 500×g. Supernatant was discarded and the cell pellet was resuspended in 1ml
960 polysome extraction buffer (PEB, 20mM Tris-HCl, pH 7.5, 100mM KCl, 5mM $MgCl_2$, 0.5%
961 Nonidet P-40, 100µg/ml CHX, 1X protease inhibitors and 1:1000 dilution of RiboLock
962 RNase inhibitor), incubated on ice for 30 minutes with occasional mixing, centrifuged at
963 12000×g for 20 minutes at $4^0$C. Total protein and RNA concentration in the clarified lysate
964 was measured by Bradford assay or Nanodrop spectrophotometry, respectively. Aliquots

965 of the lysate were used for cDNA synthesis, western blot analysis and ribosome
966 fractionation.

967 A linear 10% - 50% sucrose density gradient was prepared for ribosome fractionation,
968 one day before the polysome fractionation experiment. Stock solutions of 10%, 20%,
969 30%, 40% and 50% sucrose were prepared using 2.2M sucrose and 10x salt solution
970 (1000 mM NaCl, 200mM Tris-HCl, pH 7.5, 50 mM $MgCl_2$) in Diethyl Pyrocarbonate
971 (DEPC)-treated water. 2.2 ml of 10% stock solution of sucrose was added to the bottom
972 of a thin-wall 12.5 ml ultracentrifuge tube, followed by addition of 2.2 ml each of 20%,
973 30%, 40%, and 50% sucrose solutions. Tubes were stored at $4^0$C, overnight for
974 linearization. Next day, equal amount of clarified lysate was loaded to the top of the tubes
975 and weights were equalized. Tubes were run in a SW40Ti swinging bucket rotor at
976 190000×g for 90 minutes at $4^0$C, using a Beckman ultracentrifuge (Beckman Coulter,
977 California, USA). After centrifugation, tubes were set for fractionation in the automated
978 fraction collection unit and 24 fractions of 500 µl each were collected. Profile of RNA in
979 the fractions was captured as an indicator of different ribosome fractions (shown in Fig.
980 S6). Alternate fractions (1-23) were selected for further analysis of RNA and protein
981 distribution profiles.

982 **RNA-Immunoprecipitation assay**

983 HEK 293T cells were seeded in 60 mm dishes at a confluency of 70%. Next day, cells
984 were cotransfected with 2µg each of the pSuper-HEV IRESI and pRL-TK plasmids and
985 cells were incubated for 48 hours in DMEM media supplemented with 10% FBS in a $37^0$C
986 incubator supplied with 5% $CO_2$. Next, cells were lysed in 1ml TRI reagent and RNA was
987 extracted as per manufacturer's instructions (MRC Inc, Cincinnati, USA). 20µg of total
988 RNA was added to the binding buffer [1% Triton X-100, 150mM NaCl, 2mM EDTA (pH
989 8.0), 20mM Tris-HCl (pH 8.0)], 20 µl monoclonal anti-$m^7G$ cap antibody (Merck,
990 Massachusetts, USA) and 1µl RNAse inhibitor (RNAsin, Promega, Wisconsin, USA) was
991 added to that and samples were incubated overnight at 4°C with continuous mixing. 25
992 µl Protein G-PLUS-Agarose beads (Santa Cruz Biotechnology, Santacruz, USA) were
993 washed twice in the binding buffer and added to the samples, followed by one hour

994 incubation. Samples were centrifuged at 1000 rpm for 1 minute at $4^0$C. Supernatant
995 containing unbound RNA was collected, RNA was extracted using TRI reagent and stored
996 at -$80^0$C. Beads were washed four times in ice cold low salt wash buffer [1% SDS, 1%
997 Triton X-100, 150mM NaCl, 2mM EDTA (pH 8.0), 20mM Tris-HCl (pH 8.0)] and once in
998 high salt wash buffer [1% SDS, 1% Triton X-100, 500mM NaCl, 2mM EDTA (pH 8.0)
999 20mM Tris-HCl (pH 8.0)] and twice with Tris-EDTA buffer (pH 8.0). Finally, beads were
1000 re-suspended in the elution buffer (1% SDS, 0.1M NaHCO3), incubated for 5 minutes at
1001 $4^0$C on a rocker, followed by centrifugation at 1000 rpm for 1 minute at $4^0$C and collection
1002 of the supernatant. RNA was isolated from the supernatant using TRI reagent and all
1003 samples were simultaneously processed for QRT-PCR.

1004 **Statistics**

1005 Data are shown as mean ± standard error of mean (SEM) of three independent
1006 experiments. *P*-values were calculated by two tailed Student t-test (paired two samples
1007 for means).

1008 **Acknowledgments**

1009 RNA motif plasmid cloning backbone (pRMB) and BASU RaPID plasmid were kindly
1010 gifted by Prof. Paul Khavari. We thank Prof. Marvin Wickens for providing the Y3H assay
1011 system. We thank Prof Charles M. Rice for providing the g3A HCV replicon. We thank
1012 Mr. Dipanka Tanu Sarmah and Dr. Samrat Chatterjee for data analysis using “Enrich R”.
1013 We thank Dr. Saumya Anang and Dr. Chandru Subramani for helping in the initial
1014 experiments. We appreciate continuous support by the technical staff of RCB mass
1015 spectrometry facility in data collection. This study was funded by the Science and
1016 Engineering Research Board (SERB), Govt of India, grant to MS and THSTI core grant
1017 to MS. SK is supported by a senior research fellowship from the Department of
1018 Biotechnology, Govt of India, RV and SS are supported by a senior research fellowship
1019 from the Council of Scientific and Industrial Research, Govt of India.

1020

1021

1022 **References**


1023 1. Merrick WC, Pavitt GD. Protein synthesis initiation in eukaryotic cells. Cold Spring
1024 Harbor perspectives in biology. 2018;10(12):a033092.
1025 2. Shatsky IN, Terenin IM, Smirnova VV, Andreev DE. Cap-independent translation:
1026 what's in a name?. Trends in biochemical sciences. 2018;43(11):882-95.
1027 3. Shatsky IN, Dmitriev SE, Terenin IM, Andreev DE. Cap-and IRES-independent
1028 scanning mechanism of translation initiation as an alternative to the concept of
1029 cellular IRESs. Molecules and cells. 2010 ;30(4):285-93.
1030 4. Kaiser C, Dobrikova EY, Bradrick SS, Shveygert M, Herbert JT, Gromeier M.
1031 Activation of cap-independent translation by variant eukaryotic initiation factor 4G in
1032 vivo. RNA. 2008;14(10):2170-82.
1033 5. Trainor BM, Ghosh A, Pestov DG, Hellen CU, Shcherbik N. A translation enhancer
1034 element from black beetle virus engages yeast eIF4G1 to drive cap-independent
1035 translation initiation. Scientific reports. 2021;11(1):1-8.
1036 6. Meyer KD, Patil DP, Zhou J, Zinoviev A, Skabkin MA, Elemento O, Pestova TV, Qian
1037 SB, Jaffrey SR. 5′ UTR m6A promotes cap-independent translation. Cell.
1038 2015;163(4):999-1010.
1039 7. Meyer KD, Saletore Y, Zumbo P, Elemento O, Mason CE, Jaffrey SR.
1040 Comprehensive analysis of mRNA methylation reveals enrichment in 3′ UTRs and
1041 near stop codons. Cell. 2012;149(7):1635-46.
1042 8. Wang X, Zhao BS, Roundtree IA, Lu Z, Han D, Ma H, Weng X, Chen K, Shi H, He C.
1043 N6-methyladenosine modulates messenger RNA translation efficiency. Cell.
1044 2015;161(6):1388-99.
1045 9. Lee KM, Chen CJ, Shih SR. Regulation mechanisms of viral IRES-driven translation.
1046 Trends in microbiology. 2017;25(7):546-61.
1047 10. Brown EA, Zajac AJ, Lemon SM. In vitro characterization of an internal ribosomal
1048 entry site (IRES) present within the 5'nontranslated region of hepatitis A virus RNA:
1049 comparison with the IRES of encephalomyocarditis virus. Journal of virology.
1050 1994;68(2):1066-74.
1051 11. Ali IK, McKendrick L, Morley SJ, Jackson RJ. Activity of the hepatitis A virus IRES
1052 requires association between the cap-binding translation initiation factor (eIF4E) and
1053 eIF4G. Journal of virology. 2001;75(17):7854-63.
1054 12. Kerr CH, Jan E. Commandeering the ribosome: Lessons learned from dicistroviruses
1055 about translation. Journal of virology. 2016;90(12):5538-40.
1056 13. Khawaja A, Vopalensky V, Pospisek M. Understanding the potential of hepatitis C
1057 virus internal ribosome entry site domains to modulate translation initiation via their
1058 structure and function. Wiley Interdisciplinary Reviews: RNA. 2015;6(2):211-24.
1059 14. Pestova TV, Hellen CU. Translation elongation after assembly of ribosomes on the
1060 Cricket paralysis virus internal ribosomal entry site without initiation factors or initiator
1061 tRNA. Genes & development. 2003;17(2):181-6.

1062 15. Wilson JE, Pestova TV, Hellen CU, Sarnow P. Initiation of protein synthesis from the
1063 A site of the ribosome. Cell. 2000;102(4):511-20.
1064 16. Song Y, Mugavero J, Stauft CB, Wimmer E. Dengue and Zika virus 5′ untranslated
1065 regions harbor internal ribosomal entry site functions. MBio. 2019;10(2):e00459-19.
1066 17. Fernández-García L, Angulo J, Ramos H, Barrera A, Pino K, Vera-Otarola J, López-
1067 Lastra M. The Internal Ribosome Entry Site of Dengue Virus mRNA Is Active When
1068 Cap-Dependent Translation Initiation Is Inhibited. Journal of virology.
1069 2020;95(5):e01998-20.
1070 18. Edgil D, Polacek C, Harris E. Dengue virus utilizes a novel strategy for translation
1071 initiation when cap-dependent translation is inhibited. Journal of virology.
1072 2006;80(6):2976-86.
1073 19. Brasey A, Lopez-Lastra M, Ohlmann T, Beerens N, Berkhout B, Darlix JL, Sonenberg
1074 N. The leader of human immunodeficiency virus type 1 genomic RNA harbors an
1075 internal ribosome entry segment that is active during the G2/M phase of the cell cycle.
1076 Journal of virology. 2003;77(7):3939-49.
1077 20. Vallejos M, Deforges J, Plank TD, Letelier A, Ramdohr P, Abraham CG, Valiente-
1078 Echeverría F, Kieft JS, Sargueil B, Lopez-Lastra M. Activity of the human
1079 immunodeficiency virus type 1 cell cycle-dependent internal ribosomal entry site is
1080 modulated by IRES trans-acting factors. Nucleic acids research. 2011;39(14):6186-
1081 200.
1082 21. Ohlmann T, Lopez-Lastra M, Darlix JL. An internal ribosome entry segment promotes
1083 translation of the simian immunodeficiency virus genomic RNA. Journal of Biological
1084 Chemistry. 2000;275(16):11899-906.
1085 22. Barrera A, Olguín V, Vera-Otarola J, López-Lastra M. Cap-independent translation
1086 initiation of the unspliced RNA of retroviruses. Biochimica et Biophysica Acta (BBA)-
1087 Gene Regulatory Mechanisms. 2020;1863(9):194583.
1088 23. Shi B, Song Q, Luo X, Song J, Xia D, Xia Z, Liu M, Wang W, Wang R, Du H, Han J.
1089 Identification of cryptic putative IRESs within the ORF encoding the nonstructural
1090 proteins of the human rhinovirus 16 genome. Archives of virology.
1091 2021;166(12):3373-86.
1092 24. Shi B, Song Q, Luo X, Song J, Xia D, Xia Z, Liu M, Wang W, Wang R, Du H, Wei Q.
1093 Identification of an IRES within the coding region of the structural protein of human
1094 rhinovirus 16. Journal of Medical Virology. 2021.
1095 25. Grainger L, Cicchini L, Rak M, Petrucelli A, Fitzgerald KD, Semler BL, Goodrum F.
1096 Stress-inducible alternative translation initiation of human cytomegalovirus latency
1097 protein pUL138. Journal of virology. 2010;84(18):9472-86.
1098 26. May J, Johnson P, Saleem H, Simon AE. A sequence-independent, unstructured
1099 internal ribosome entry site is responsible for internal expression of the coat protein
1100 of Turnip crinkle virus. Journal of Virology. 2017;91(8):e02421-16.

1101 27. Nair VP, Anang S, Subramani C, Madhvi A, Bakshi K, Srivastava A, Nayak B, CT RK,
1102 Surjit M. Endoplasmic reticulum stress induced synthesis of a novel viral factor
1103 mediates efficient replication of genotype-1 hepatitis E virus. PLoS pathogens.
1104 2016;12(4):e1005521.
1105 28. Ramanathan M, Majzoub K, Rao DS, Neela PH, Zarnegar BJ, Mondal S, Roth JG,
1106 Gai H, Kovalski JR, Siprashvili Z, Palmer TD. RNA–protein interaction detection in
1107 living cells. Nature methods. 2018;15(3):207-12.
1108 29. Verma R, Saha S, Kumar S, Mani S, Maiti TK, Surjit M. RNA-Protein Interaction
1109 Analysis of SARS-CoV-2 5′ and 3′ Untranslated Regions Reveals a Role of
1110 Lysosome-Associated Membrane Protein-2a during Viral Infection. Msystems.
1111 2021;6(4):e00643-21.
1112 30. Koh YY, Wickens M. Determining the RNA specificity and targets of RNA-binding
1113 proteins using a three-hybrid system. InMethods in enzymology. 2014; (Vol. 539:163-
1114 181). Academic Press.
1115 31. Cho SK, Kang IH, Carr T, Hannapel DJ. Using the yeast three-hybrid system to
1116 identify proteins that interact with a phloem-mobile mRNA. Frontiers in Plant Science.
1117 2012;3:189.
1118 32. Pacheco A, Reigadas S, Martínez-Salas E. Riboproteomic analysis of polypeptides
1119 interacting with the internal ribosome-entry site element of foot-and-mouth disease
1120 viral RNA. Proteomics. 2008;8(22):4782-90.
1121 33. Otto GA, Lukavsky PJ, Lancaster AM, Sarnow P, Puglisi JD. Ribosomal proteins
1122 mediate the hepatitis C virus IRES–HeLa 40S interaction. RNA. 2002;8(7):913-23.
1123 34. Godet AC, David F, Hantelys F, Tatin F, Lacazette E, Garmy-Susini B, Prats AC.
1124 IRES trans-acting factors, key actors of the stress response. International Journal of
1125 Molecular Sciences. 2019;20(4):924.
1126 35. Kappel K, Jarmoskaite I, Vaidyanathan PP, Greenleaf WJ, Herschlag D, Das R. Blind
1127 tests of RNA–protein binding affinity prediction. Proceedings of the National Academy
1128 of Sciences. 2019;116(17):8336-41.
1129 36. Yan Y, Zhang D, Zhou P, Li B, Huang SY. HDOCK: a web server for protein–protein
1130 and protein–DNA/RNA docking based on a hybrid strategy. Nucleic acids research.
1131 2017;45(W1):W365-73.
1132 37. Jia D, Cai L, He H, Skogerbø G, Li T, Aftab MN, Chen R. Systematic identification of
1133 non-coding RNA 2, 2, 7-trimethylguanosine cap structures in Caenorhabditis elegans.
1134 BMC molecular biology. 2007;8(1):1-9.
1135 38. Panda AC, Martindale JL, Gorospe M. Polysome fractionation to analyze mRNA
1136 distribution profiles. Bio-protocol. 2017;7(3).
1137 39. Chassé H, Boulben S, Costache V, Cormier P, Morales J. Analysis of translation
1138 using polysome profiling. Nucleic acids research. 2017;45(3):e15-e15.
1139 40. Davis TL, Walker JR, Campagna-Slater V, Finerty Jr PJ, Paramanathan R, Bernstein
1140 G, MacKenzie F, Tempel W, Ouyang H, Lee WH, Eisenmesser EZ. Structural and

1141 biochemical characterization of the human cyclophilin family of peptidyl-prolyl
1142 isomerases. PLoS biology. 2010;8(7):e1000439.
1143 41. Nimgaonkar I, Ding Q, Schwartz RE, Ploss A. Hepatitis E virus: advances and
1144 challenges. Nature Reviews Gastroenterology & Hepatology. 2018;15(2):96-110.
1145 42. Surjit M, Liu B, Chow VT, Lal SK. The nucleocapsid protein of severe acute
1146 respiratory syndrome-coronavirus inhibits the activity of cyclin-cyclin-dependent
1147 kinase complex and blocks S phase progression in mammalian cells. Journal of
1148 Biological Chemistry. 2006;281(16):10669-81.
1149 43. Nagashima S, Takahashi M, Tanaka T, Yamada K, Nishizawa T, Okamoto H. A PSAP
1150 motif in the ORF3 protein of hepatitis E virus is necessary for virion release from
1151 infected cells. Journal of general virology. 2011;92(2):269-78.
1152 44. Ding Q, Heller B, Capuccino JM, Song B, Nimgaonkar I, Hrebikova G, Contreras JE,
1153 Ploss A. Hepatitis E virus ORF3 is a functional ion channel required for release of
1154 infectious particles. Proceedings of the National Academy of Sciences.
1155 2017;114(5):1147-52.
1156 45. Xu LD, Zhang F, Peng L, Luo WT, Chen C, Xu P, Huang YW. Stable expression of a
1157 hepatitis E Virus (HEV) RNA replicon in two mammalian cell lines to assess
1158 mechanism of innate immunity and antiviral response. Frontiers in microbiology.
1159 2020:3093.
1160 46. Hinton TM, Li F, Crabb BS. Internal ribosomal entry site-mediated translation initiation
1161 in equine rhinitis A virus: similarities to and differences from that of foot-and-mouth
1162 disease virus. Journal of Virology. 2000;74(24):11708-16.
1163 47. Russo G, Cuccurese M, Monti G, Russo A, Amoresano A, Pucci P, Pietropaolo C.
1164 Ribosomal protein L7a binds RNA through two distinct RNA-binding domains.
1165 Biochemical Journal. 2005;385(1):289-99.
1166 48. Martel G, Hamet P, Tremblay J. GREBP, a cGMP-response element-binding protein
1167 repressing the transcription of natriuretic peptide receptor 1 (NPR1/GCA). Journal of
1168 Biological Chemistry. 2010;285(27):20926-39.
1169 49. Babiano R, Gamalinda M, Woolford Jr JL, de la Cruz J. Saccharomyces cerevisiae
1170 ribosomal protein L26 is not essential for ribosome assembly and function. Molecular
1171 and cellular biology. 2012;32(16):3228-41.
1172 50. Chen J, Guo K, Kastan MB. Interactions of nucleolin and ribosomal protein L26
1173 (RPL26) in translational control of human p53 mRNA. Journal of Biological Chemistry.
1174 2012;287(20):16467-76.
1175 51. Takagi M, Absalon MJ, McLure KG, Kastan MB. Regulation of p53 translation and
1176 induction after DNA damage by ribosomal protein L26 and nucleolin. Cell.
1177 2005;123(1):49-63.
1178 52. Wilson-Edell KA, Kehasse A, Scott GK, Yau C, Rothschild DE, Schilling B, Gabriel
1179 BS, Yevtushenko MA, Hanson IM, Held JM, Gibson BW. RPL24: a potential

1180 therapeutic target whose depletion or acetylation inhibits polysome assembly and
1181 cancer cell growth. Oncotarget. 2014;5(13):5165.
1182 53. Wang S, Huang J, He J, Wang A, Xu S, Huang SF, Xiao S. RPL41, a small ribosomal
1183 peptide deregulated in tumors, is essential for mitosis and centrosome integrity.
1184 Neoplasia. 2010;12(3):284-IN8.
1185 54. Subramani C, Nair VP, Anang S, Mandal SD, Pareek M, Kaushik N, Srivastava A,
1186 Saha S, Shalimar, Nayak B, Ranjith-Kumar CT. Host-virus protein interaction network
1187 reveals the involvement of multiple host processes in the life cycle of hepatitis E virus.
1188 MSystems. 2018;3(1):e00135-17.
1189 55. Hartman TR, Qian S, Bolinger C, Fernandez S, Schoenberg DR, Boris-Lawrie K. RNA
1190 helicase A is necessary for translation of selected messenger RNAs. Nature structural
1191 & molecular biology. 2006;13(6):509-16.
1192 56. Bolinger C, Sharma A, Singh D, Yu L, Boris-Lawrie K. RNA helicase A modulates
1193 translation of HIV-1 and infectivity of progeny virions. Nucleic acids research.
1194 2010;38(5):1686-96.
1195 57. Bolinger C, Yilmaz A, Hartman TR, Kovacic MB, Fernandez S, Ye J, Forget M, Green
1196 PL, Boris-Lawrie K. RNA helicase A interacts with divergent lymphotropic retroviruses
1197 and promotes translation of human T-cell leukemia virus type 1. Nucleic acids
1198 research. 2007;35(8):2629-42.
1199 58. Shi RZ, Pan YQ, Xing L. RNA Helicase A Regulates the Replication of RNA Viruses.
1200 Viruses. 2021;13(3):361.
1201 59. Paingankar MS, Arankalle VA. Identification and characterization of cellular proteins
1202 interacting with Hepatitis E virus untranslated regions. Virus research. 2015;208:98-
1203 109.
1204 60. Koh HR, Xing L, Kleiman L, Myong S. Repetitive RNA unwinding by RNA helicase A
1205 facilitates RNA annealing. Nucleic acids research. 2014;42(13):8556-64.
1206 61. Zhang S, Grosse F. Domain structure of human nuclear DNA helicase II (RNA
1207 helicase A). Journal of Biological Chemistry. 1997;272(17):11487-94.
1208 62. Yin M, Cheng M, Liu C, Wu K, Xiong W, Fang J, Li Y, Zhang B. HNRNPA2B1 as a
1209 trigger of RNA switch modulates the miRNA-mediated regulation of CDK6. Iscience.
1210 2021;24(11):103345.
1211 63. Pingale KD, Kanade GD, Karpe YA. Heterogeneous Nuclear Ribonucleoproteins
1212 Participate in Hepatitis E Virus Replication. Journal of Molecular Biology. 2020 Mar
1213 27;432(7):2369-87.
1214 64. Wang X, Lu Z, Gomez A, Hon GC, Yue Y, Han D, Fu Y, Parisien M, Dai Q, Jia G,
1215 Ren B. N6-methyladenosine-dependent regulation of messenger RNA stability.
1216 Nature. 2014;505(7481):117-20.
1217 65. Du H, Zhao Y, He J, Zhang Y, Xi H, Liu M, Ma J, Wu L. YTHDF2 destabilizes m6A-
1218 containing RNA through direct recruitment of the CCR4–NOT deadenylase complex.
1219 Nature communications. 2016;7(1):1-1.

1220 66. Kaul G, Pattan G, Rafeequi T. Eukaryotic elongation factor-2 (eEF2): its regulation
1221 and peptide chain elongation. Cell biochemistry and function. 2011;29(3):227-34.
1222 67. Mattijssen S, Arimbasseri AG, Iben JR, Gaidamakov S, Lee J, Hafner M, Maraia RJ.
1223 LARP4 mRNA codon-tRNA match contributes to LARP4 activity for ribosomal protein
1224 mRNA poly (A) tail length protection. Elife. 2017;6:e28889.
1225 68. Mattijssen S, Iben JR, Li T, Coon SL, Maraia RJ. Single molecule poly (A) tail-seq
1226 shows LARP4 opposes deadenylation throughout mRNA lifespan with most impact
1227 on short tails. Elife. 2020;9:e59186.
1228 69. Yang R, Gaidamakov SA, Xie J, Lee J, Martino L, Kozlov G, Crawford AK, Russo AN,
1229 Conte MR, Gehring K, Maraia RJ. La-related protein 4 binds poly (A), interacts with
1230 the poly (A)-binding protein MLLE domain via a variant PAM2w motif, and can
1231 promote mRNA stability. Molecular and cellular biology. 2011;31(3):542-56.
1232 70. Meares GP, Zmijewska AA, Jope RS. HSP105 interacts with GRP78 and GSK3 and
1233 promotes ER stress-induced caspase-3 activation. Cellular signalling.
1234 2008;20(2):347-58.
1235 71. Mkrtchian S, Fang C, Hellman U, Ingelman-Sundberg M. A stress-inducible rat liver
1236 endoplasmic reticulum protein, ERp29. European journal of biochemistry.
1237 1998;251(1-2):304-13.
1238 72. Hotokezaka Y, Katayama I, van Leyen K, Nakamura T. GSK-3β-dependent
1239 downregulation of γ-taxilin and αNAC merge to regulate ER stress responses. Cell
1240 death & disease. 2015;6(4):e1719-.
1241 73. Cairrao F, Santos CC, Le Thomas A, Marsters S, Ashkenazi A, Domingos PM.
1242 Pumilio protects Xbp1 mRNA from regulated Ire1-dependent decay. Nature
1243 Communications. 2022;13(1):1-3.
1244 74. Saeed M, Scheel TK, Gottwein JM, Marukian S, Dustin LB, Bukh J, Rice CM. Efficient
1245 replication of genotype 3a and 4a hepatitis C virus replicons in human hepatoma
1246 cells. Antimicrobial agents and chemotherapy. 2012;56(10):5365-73.
1247 75. Surjit M, Jameel S, Lal SK. The ORF2 protein of hepatitis E virus binds the 5′ region
1248 of viral RNA. Journal of virology. 2004;78(1):320-8.
1249 76. Zuker M. Mfold web server for nucleic acid folding and hybridization prediction.
1250 Nucleic acids research. 2003;31(13):3406-15.
1251 77. Kuleshov MV, Jones MR, Rouillard AD, Fernandez NF, Duan Q, Wang Z, Koplev S,
1252 Jenkins SL, Jagodnik KM, Lachmann A, McDermott MG. Enrichr: a comprehensive
1253 gene set enrichment analysis web server 2016 update. Nucleic acids research.
1254 2016;44(W1):W90-7.

1255

1256

1257

1258 **Supplementary Figures and Tables**

Supplementary Figure 1

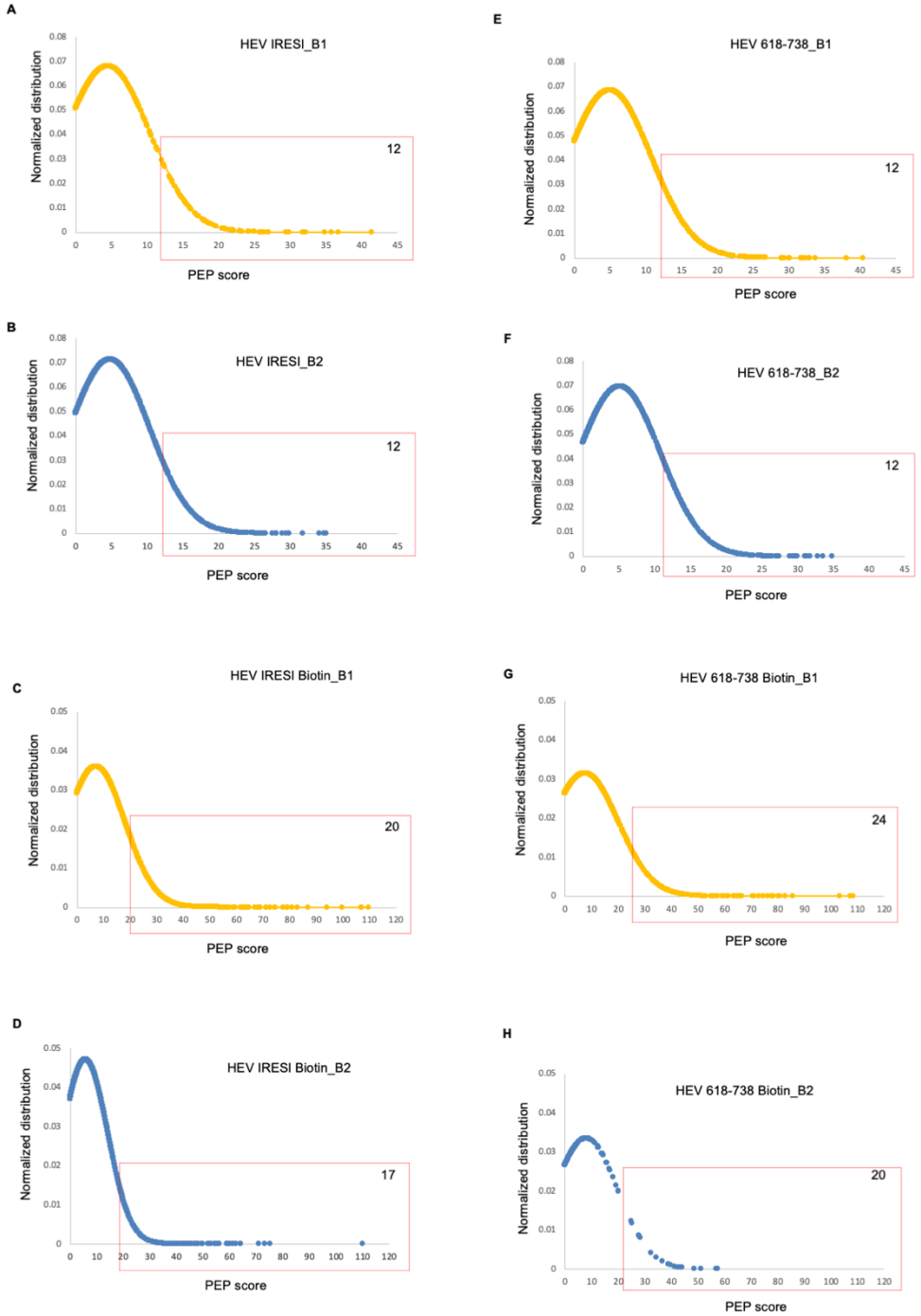


1259

1260

1261 **Figure S1. Normalized distribution plots of the peptides identified by LC-MS/MS.**

1262 (A-H) Normalized distribution plots showing all peptides identified in LC-MS/MS against their
1263 respective PEP scores. B1 and B2 denote biological replicates of the same samples. PEP score
1264 range considered for protein identification is shown by a dotted-lined box.

1265

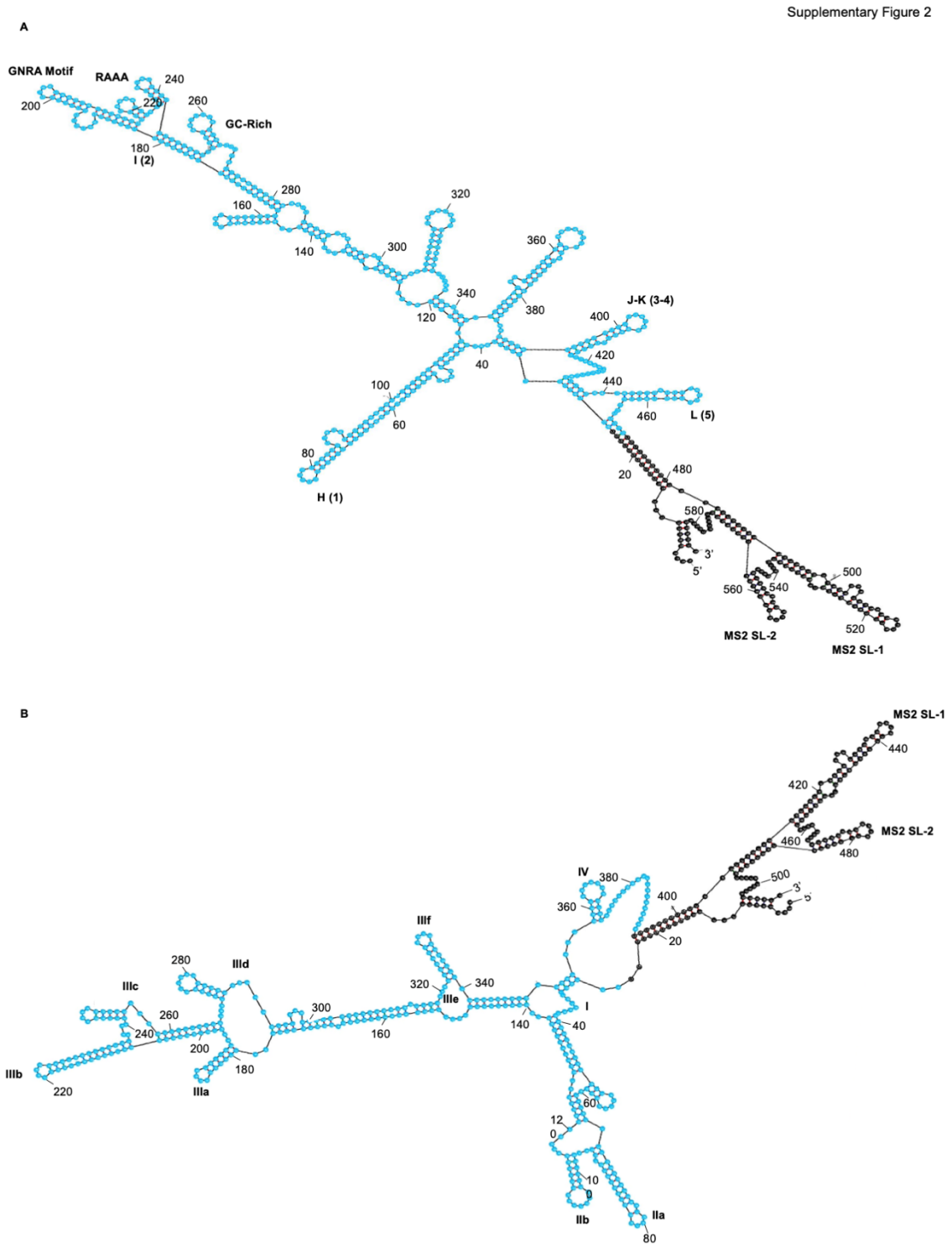


1266

1267 **Figure S2. Predicted secondary structure of the FMDV and HCV IRES RNA.**

1268 (A) Predicted secondary structure of the FMDV IRES RNA (shown in blue) fused to the MS2-
1269 coat protein-binding RNA. MS2 SL-1 and MS2 SL-2 represent MS2 coat proteinbinding RNA
1270 motifs. Five SLs of the IRES are numbered H-L (1-5) and span positions 26113, 114-344, 343-
1271 418 and 417- 470, respectively. GNRA, RAAA, GC-rich motifs are as indicated. (B) Predicted
1272 secondary structure of the HCV IRES RNA (shown in blue) fused to the MS2-RNA. MS2 SL-1
1273 and MS2 SL-2 represent MS2 coat protein-binding RNA motifs. Four stem-loops (SL) of the
1274 IRES are numbered as I, II, III (a-e) and IV.

1275

1276

Supplementary Figure 3

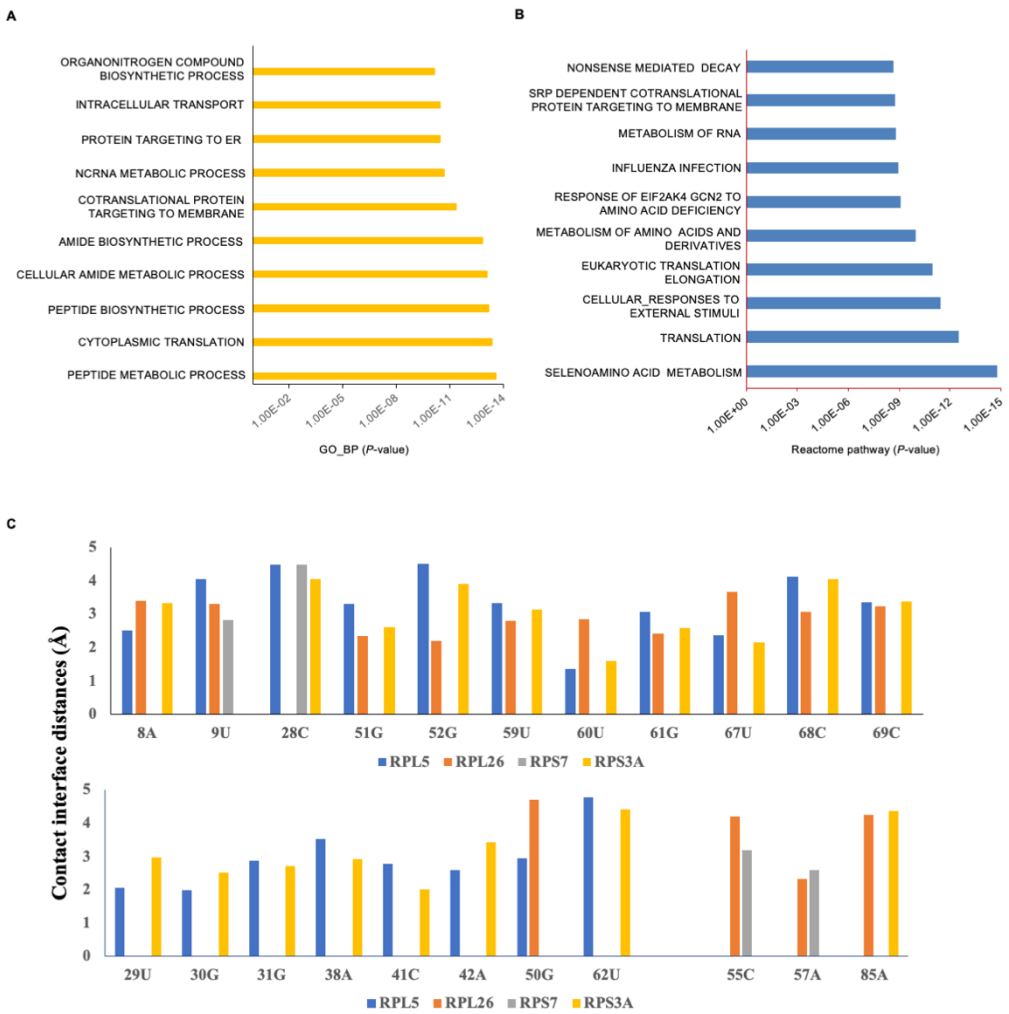


1277

1278 **Figure S3. Bioinformatics analysis of the HEV IRESI RNA-host protein interaction.**

1279 (A) Graphical representation of the top 10 Biological processes (sorted by P-values) enriched in
1280 the HEV IRESI RNA-protein interactome, analyzed by the GSEA tool (B) Graphical
1281 representation of the top 10 Reactome pathways (sorted by P-values) enriched in the HEV
1282 IRESI RNA-protein interactome, analyzed by the GSEA tool. (C) Quantitative pair-wise contact
1283 interface distance calculation between the HEV IRESI RNA and the indicated ribosomal
1284 proteins. The pair-wise interface residues contacts (measured in the form of distance in Å) was
1285 calculated for each complex. The common contact nucleotides of the HEV IRESI RNA are
1286 shown in the upper and lower panels, respectively.

1287

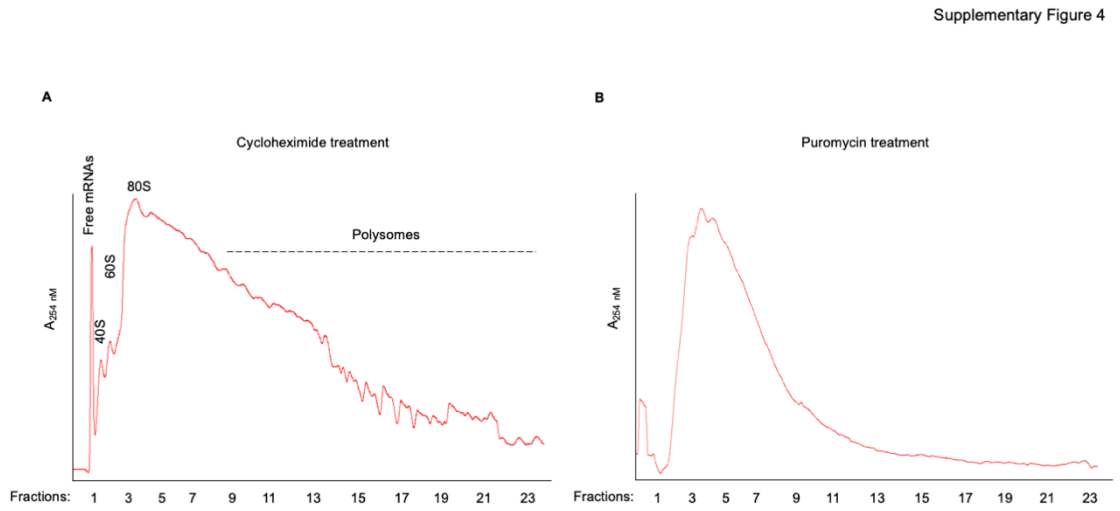


1288

1289 **Figure S4. Ribosome fractionation profiles of cycloheximide or puromycin treated**
1290 **Huh7 cells.**

1291 (A) HEK 293T cells were treated with cycloheximide for 30 min, followed by preparation of the
1292 cytosolic extract and ultracentrifugation on 10-50% sucrose gradients. Equal volume fractions
1293 were collected from the top in an automated fraction collector. Real-time profile of the RNA
1294 content in each fraction was measured at $A_{254nm}$ and the plot generated by the application
1295 software is shown. Peaks corresponding to free mRNAs, 40S, 60S, 80S ribosome and
1296 polysome fractions are indicated based on earlier reports. (B) HEK 293T cells were treated with
1297 puromycin for 30 min, followed by preparation of the cytosolic extract and ultracentrifugation on
1298 10-50% sucrose gradients. Equal volume fractions were collected from the top in an automated

1299 fraction collector. Real-time profile of the RNA content in each fraction was measured at $A_{254nm}$
1300 and the plot generated by the application software is shown.

1301

**Table S1. List of the HEV IRESI RNA interaction partners, identified by RaPID-LC-MS-MS**

| Protein name | prot_desc | prot_score | No. of unique peptide | pep_score |
|---|---|---|---|---|
| EF2 | Elongation factor 2 | 1568 | 6 | 59.63 |
| TBA3C | Tubulin alpha-3C/D chain | 929 | 1 | 24.2 |
| SYTC | Threonyl-tRNA synthetase, cytoplasmic | 285 | 5 | 17.17 |
| ROA2 | Heterogeneous nuclear ribonucleoproteins A2/B1 | 285 | 2 | 35.14 |
| RL7A | 60S ribomal protein L7a | 262 | 3 | 19 |
| BA2L2 | Protein BAT2-like 2 | 75 | 1 | 74.55 |
| NUFP2 | Nuclear fragile X mental retardation-interacting protein 2 | 75 | 1 | 46.91 |
| SYVC | Valyl-tRNA synthetase | 56 | 8 | 18.02 |
| DHX9 | ATP-dependent RNA helicase A | 53 | 7 | 42.62 |
| SYTC2 | Probable threonyl-tRNA synthetase 2, cytoplasmic | 53 | 5 | 17.17 |
| ARP19 | cAMP-regulated phphoprotein 19 | 53 | 1 | 52.79 |
| ENSA | Alpha-endulfine | 53 | 1 | 52.79 |
| RL24 | 60S ribomal protein L24 | 53 | 1 | 35.28 |
| HS105 | Heat shock protein 105 kDa | 50 | 6 | 20.75 |
| CATA | Catalase | 49 | 2 | 49.14 |
| DDX10 | Probable ATP-dependent RNA helicase DDX10 | 42 | 9 | 42.18 |
| LARP4 | La-related protein 4 | 42 | 1 | 41.97 |
| MIMIT | Mimitin, mitochondrial | 41 | 1 | 41.09 |
| DBNL | Drebrin-like protein | 39 | 1 | 36.56 |
| LBR | Lamin-B receptor | 38 | 1 | 37.78 |
| AIMP1 | Aminoacyl tRNA synthetase complex-interacting multifunctional protein 1 | 37 | 3 | 20.08 |
| NSF | Vesicle-fusing ATPase | 37 | 1 | 19 |

| | | | | |
|---|---|---|---|---|
| VW5B1 | von Willebrand factor A domain-containing protein 5B1 | 35 | 5 | 40.75 |
| CEA16 | Carcinoembryonic antigen-related cell adhesion molecule 16 | 35 | 1 | 34.88 |
| CCD65 | Coiled-coil domain-containing protein 65 | 34 | 5 | 33.67 |
| CN043 | Uncharacterized protein C14orf43 | 34 | 4 | 33.93 |
| PUM1 | Pumilio homolog 1 | 34 | 2 | 34.22 |
| TXLNG | Gamma-taxilin | 33 | 10 | 33.34 |
| RFA1 | Replication protein A 70 kDa DNA-binding subunit | 33 | 4 | 32.54 |
| ARSJ | Arylsulfatase J | 33 | 1 | 32.32 |
| CCD67 | Coiled-coil domain-containing protein 67 | 32 | 8 | 32.5 |
| BIVM | Basic immunoglobulin-like variable motif-containing protein | 32 | 3 | 32.47 |
| YTHD2 | YTH domain family protein 2 | 32 | 2 | 32.45 |
| RSBNL | Round spermatid basic protein 1-like protein | 32 | 1 | 32.09 |
| SPD2A | SH3 and PX domain-containing protein 2A | 32 | 1 | 31.88 |
| UBAP2 | Ubiquitin-associated protein 2 | 32 | 1 | 32.35 |
| GLSK | Glutaminase kidney isoform, mitochondrial | 31 | 1 | 30.81 |
| MRE11 | Double-strand break repair protein MRE11A | 31 | 1 | 31.09 |
| PRAF3 | PRA1 family protein 3 | 31 | 1 | 20.25 |
| CENPP | Centromere protein P | 30 | 1 | 29.73 |
| ERP29 | Endoplasmic reticulum resident protein 29 | 30 | 1 | 23.18 |
| LASP1 | LIM and SH3 domain protein 1 | 30 | 1 | 29.73 |
| TM59L | Transmembrane protein 59-like | 30 | 1 | 29.73 |
| COL10 | Collectin-10 | 29 | 3 | 29.32 |
| ZYX | Zyxin | 29 | 2 | 29.49 |
| GATS | Putative protein GATS | 29 | 1 | 29.38 |
| PPN | Papilin | 29 | 1 | 28.77 |
| SC31A | Protein transport protein Sec31A | 29 | 1 | 29.47 |
| SYQ | Glutaminyl-tRNA synthetase | 29 | 1 | 29.38 |
| PAPS2 | Bifunctional 3~-phphoadenine 5~-phphulfate synthase 2 | 28 | 3 | 27.81 |

| | | | | |
|---|---|---|---|---|
| K0649 | Protein KIAA0649 | 28 | 2 | 27.59 |
| NUP88 | Nuclear pore complex protein Nup88 | 28 | 2 | 25.32 |
| NALDL | N-acetylated-alpha-linked acidic dipeptidase-like protein | 28 | 1 | 27.97 |
| VPS39 | Vam6/Vps39-like protein | 28 | 1 | 28.29 |
| ZC12C | Probable ribonuclease ZC3H12C | 28 | 1 | 27.67 |
| LRRF2 | Leucine-rich repeat flightless-interacting protein 2 | 27 | 5 | 27.36 |
| M4K4 | Mitogen-activated protein kinase kinase kinase kinase 4 | 27 | 5 | 19.92 |
| F195A | Protein FAM195A | 27 | 2 | 26.9 |
| MDN1 | Midasin | 26 | 2 | 17.57 |
| ACRBP | Acrin-binding protein | 26 | 1 | 26.38 |
| UBP7 | Ubiquitin carboxyl-terminal hydrolase 7 | 26 | 1 | 26.35 |
| GRM7 | Metabotropic glutamate receptor 7 | 25 | 3 | 25.19 |
| CHMP5 | Charged multivesicular body protein 5 | 25 | 1 | 25.45 |
| MGAP | MAX gene-associated protein | 24 | 13 | 21.31 |
| ATP7A | Copper-transporting ATPase 1 | 24 | 6 | 24.32 |
| TRM1 | N(2),N(2)-dimethylguanine tRNA methyltransferase | 24 | 4 | 24.25 |
| CND3 | Condensin complex subunit 3 | 24 | 1 | 24.31 |
| K2C74 | Keratin, type II cytkeletal 74 | 24 | 1 | 23.82 |
| QTRD1 | Queuine tRNA-ribyltransferase subunit QTRTD1 | 24 | 1 | 24.1 |
| S28A3 | Solute carrier family 28 member 3 | 24 | 1 | 23.51 |
| ZN469 | Zinc finger protein 469 | 24 | 1 | 24.29 |
| DYRK3 | Dual specificity tyrine-phphorylation-regulated kinase 3 | 23 | 1 | 23.42 |
| EZH1 | Histone-lysine N-methyltransferase EZH1 | 23 | 1 | 23.02 |
| EZH2 | Histone-lysine N-methyltransferase EZH2 | 23 | 1 | 23.02 |
| FA81A | Protein FAM81A | 23 | 1 | 22.56 |
| MMP12 | Macrophage metalloelastase | 23 | 1 | 23.36 |
| FA98A | Protein FAM98A | 22 | 5 | 22.05 |
| XPO4 | Exportin-4 | 22 | 3 | 20.68 |
| TEX15 | Testis-expressed sequence 15 protein | 22 | 2 | 21.88 |
| CF050 | Uncharacterized protein C6orf50 | 22 | 1 | 22.14 |
| NIN | Ninein | 22 | 1 | 22.37 |

| | | | | |
|---|---|---|---|---|
| VP37A | Vacuolar protein sorting-associated protein 37A | 22 | 1 | 21.61 |
| CB067 | Uncharacterized protein C2orf67 | 21 | 10 | 21.12 |
| EDRF1 | Erythroid differentiation-related factor 1 | 21 | 8 | 19.38 |
| YE031 | Transmembrane protein ENSP00000382582 | 21 | 5 | 21.06 |
| TT21A | Tetratricopeptide repeat protein 21A | 21 | 4 | 17.03 |
| ABCG2 | ATP-binding cassette sub-family G member 2 | 21 | 2 | 21.29 |
| NMD3B | Glutamate [NMDA] receptor subunit 3B | 21 | 2 | 20.88 |
| TEX28 | Testis-specific protein TEX28 | 21 | 2 | 20.57 |
| ABHD6 | Monoacylglycerol lipase ABHD6 | 21 | 1 | 21.27 |
| ACBG2 | Long-chain-fatty-acid--CoA ligase ACSBG2 | 21 | 1 | 20.91 |
| COLQ | Acetylcholinesterase collagenic tail peptide | 21 | 1 | 21.16 |
| GMFB | Glia maturation factor beta | 21 | 1 | 21.34 |
| NIT1 | Nitrilase homolog 1 | 21 | 1 | 21.38 |
| S26A7 | Anion exchange transporter | 21 | 1 | 20.95 |
| YE015 | Ankyrin repeat and death domain-containing protein | 21 | 1 | 24.63 |
| ZN236 | Zinc finger protein 236 | 21 | 1 | 20.51 |
| AGAP2 | Arf-GAP with GTPase, ANK repeat and PH domain-containing protein 2 | 20 | 4 | 20.09 |
| SYLC | Leucyl-tRNA synthetase, cytoplasmic | 20 | 4 | 18.18 |
| DC1I1 | Cytoplasmic dynein 1 intermediate chain 1 | 20 | 2 | 19.91 |
| HPHL1 | Hephaestin-like protein 1 | 20 | 2 | 20.04 |
| MYPC2 | Myin-binding protein C, fast-type | 20 | 1 | 20.25 |
| PRAF2 | PRA1 family protein 2 | 20 | 1 | 20.25 |
| CO4A1 | Collagen alpha-1(IV) chain | 19 | 9 | 19.05 |
| PGS2 | Decorin | 19 | 5 | 19.27 |
| RASA1 | Ras GTPase-activating protein 1 | 19 | 5 | 19.15 |
| RBL1 | Retinoblastoma-like protein 1 | 19 | 5 | 19.69 |
| CO033 | Uncharacterized protein C15orf33 | 19 | 4 | 22.99 |
| DYH9 | Dynein heavy chain 9, axonemal | 18 | 18 | 18.01 |
| LKAP | Limkain-b1 | 18 | 14 | 17.68 |

| | | | | |
|---|---|---|---|---|
| TRPM3 | Transient receptor potential cation channel subfamily M member 3 | 18 | 9 | 22.95 |
| AKT1 | RAC-alpha serine/threonine-protein kinase | 18 | 1 | 17.93 |
| CCD34 | Coiled-coil domain-containing protein 34 | 16 | 1 | 20.12 |
| CNN1 | Calponin-1 | 16 | 1 | 20.87 |
| KNTC1 | Kinetochore-associated protein 1 | 15 | 8 | 18.24 |

1313

**Table S2. Summary of human fetal liver library screening by the Y3H assay to identify the host factors that interact with the HEV IRESI element** 1314

| Description | No. of Colonies |
|---|---|
| Number of clones screened | $4 \times 10^6$ 1316 |
| Number of colonies on ($LUH^-$+10mM 3AT) | 395 1317 |
| Number of colonies containing human liver cDNA insert | 285 |
| Number of colonies containing unique cDNA insert | 75 1318 |
| Unique protein coding sequences in frame with the AD | 8 1319 |
| Number of positive clones upon retransformation of the p3HR2-HEV IRESI and the isolated liver library clone | 8 1320 |

1321

**Table S3. Analysis of interaction of the HEV IRESI RNA-interacting host proteins (found in Y3H library screening) with the FMDV and HCV IRES RNA[a]**

| Name of the host protein | HEV IRESI | FMDV IRES | HCV IRES |
|---|---|---|---|
| GREBP | +++ | + | + |
| PPIG | + | - | +++ |
| RPL5 | +++ | - | + |
| RPL26 | ++ | - | +++ |
| RPL41 | +++ | - | - |
| RPS3A | +++ | +++ | +++ |
| RPS7 | +++ | - | + |
| RPS15A | +++ | - | - |

[a] +++ : Strong Interaction; + : weak interaction; - : No interaction

1322